

ORIGINAL RESEARCH

Open Access



# Synergistically enhancing nitrate reduction into N<sub>2</sub> in water by N-doped Pd–Cu biochar bimetallic single-atom electrocatalysis

Lihao Zhang<sup>1,2</sup>, Yuqing Wu<sup>1</sup>, Zongqiang Zhu<sup>1,4\*</sup> , Yinian Zhu<sup>1,2,3\*</sup>, Yi Dong<sup>1</sup>, Meina Liang<sup>1,2</sup> and Huan Deng<sup>1,2</sup>

## Abstract

Noble metal materials have been identified as high efficiency catalysts for electrocatalytic reduction of nitrate, and the synthesis and manufacture of high catalytic activity and environmentally friendly catalysts of activating hydrogen for water purification applications is extremely attractive. In this work, the Pd–Cu single-atom catalysts (Pd–Cu–N–BC) were first prepared by direct growth of Pd–Cu single-atom on bamboo biochar by regulating the concentration of precursors and doping method, and then enhanced electrocatalytic reduction nitrate performance and N<sub>2</sub> generation. The results showed that Pd–Cu–N–BC displayed excellent catalytic activity and reusability in electrocatalytic reduction nitrate with a low potential of 0.47 V vs. RHE (@10 mA cm<sup>-2</sup>). The maximum nitrate removal efficiency and N<sub>2</sub> generation could reach about 100% and 72.32% within 180 min, respectively. The density functional theory (DFT) calculations confirmed that Cu atoms could catalyze the electrochemical reduction of nitrate to nitrite, and Pd atoms anchored in the nitrogen-doped biochar (N-BC) lattice could catalyze electrochemical reduction of nitrite to N<sub>2</sub> involving the formation of hydrogen radical (H<sup>\*</sup>). The characterization results of XANES showed that electronic synergistic effect between Pd and Cu single atoms significantly promotes the N<sub>2</sub> production through hydrogenation while inhibiting the generation of byproducts, leading to significantly enhanced electrocatalytic reduction of nitrate to N<sub>2</sub>. Finally, Pd–Cu–N–BC was designed as a 3D particle electrode for enhanced electrocatalytic reduction of nitrate, exhibiting excellent stability and reusability, which could be considered as a suitable candidate for applications in the remediation of nitrate contamination.

## Highlights

1. Excellent-active and N<sub>2</sub> selective Pd–Cu–BC SACs were prepared through bamboo biochar;
2. A typical three-dimensional electrocatalytic NO<sub>3</sub>-N reduction system was proposed;
3. N doping could reasonably modulate the electronic structure of Pd and Cu sites;
4. Free radical (H<sup>\*</sup>) played an important role in the nitrate electro-chemical reduction;
5. Synergy between Pd and Cu in SACs could enhance NO<sub>3</sub>-N removal and N<sub>2</sub> generation.

Handling editor: Xiangke Wang

\*Correspondence:

Zongqiang Zhu  
zhuzongqiang@glut.edu.cn  
Yinian Zhu  
zhuyinian@glut.edu.cn

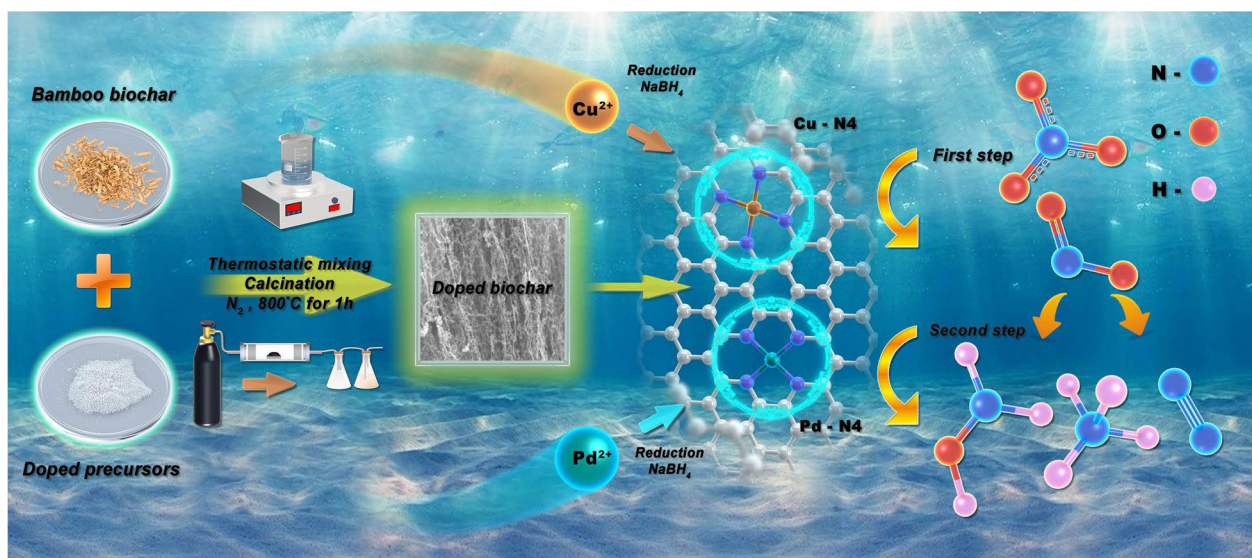
Full list of author information is available at the end of the article



© The Author(s) 2024. **Open Access** This article is licensed under a Creative Commons Attribution 4.0 International License, which permits use, sharing, adaptation, distribution and reproduction in any medium or format, as long as you give appropriate credit to the original author(s) and the source, provide a link to the Creative Commons licence, and indicate if changes were made. The images or other third party material in this article are included in the article's Creative Commons licence, unless indicated otherwise in a credit line to the material. If material is not included in the article's Creative Commons licence and your intended use is not permitted by statutory regulation or exceeds the permitted use, you will need to obtain permission directly from the copyright holder. To view a copy of this licence, visit <http://creativecommons.org/licenses/by/4.0/>.

**Keywords** Bamboo biochar, Single atom catalyst, Electrocatalytic denitration, Hydrogen evolution reaction, Density functional theory

### Graphical Abstract



## 1 Introduction

Nitrate pollution, resulting in an increasing trend in nitrate concentrations in the groundwater and surface water, has become a more and more noticeable issue around the world in recent decades (Zhang et al. 2018; Holmes et al. 2019; Fadhullah et al. 2020; Zhang et al. 2021). The increase of nitrate concentration will have a serious effect on the natural ecosystems, leading to eutrophication and hypoxia, etc. (Carey et al. 2011; Hwang et al. 2011; Su et al. 2017; Hoagland et al. 2019; Khan et al. 2023). The accumulation and increase of nitrate in drinking water is also harmful to the health of humans and animals, such as methemoglobinemia, spontaneous abortion and gastric cancer (Knobeloch et al. 2000; Ward et al. 2005; Zhai et al. 2017). For the sake of people's health, an upper content of NO<sub>3</sub>-N in drinking water, stipulated by the World Health Organization, cannot exceed 10 mg L<sup>-1</sup>. Thereby, identifying the sources and transformation of nitrate is crucial for avoiding pollution and controlling water quality effectively. For a long time, the development of efficient NO<sub>3</sub>-N removal technologies has attracted widespread attention in order to prevent and remediate nitrate pollution.

Up to now, various treatment methods have been explored for nitrate removal including physical, biological, and chemical reduction methods, and so on (Koparal

et al. 2002; Cheng et al. 2005; Wang et al. 2016). Physical methods are mainly membrane-based separation techniques, including ion exchange, reverse osmosis, and electrodialysis, which have the advantages of the automation and the high removal efficiency. However, high operating cost and limited membrane life preclude their wide application (Koparal et al. 2002; Ozturk et al. 2004; Ruangchainikom et al. 2006; Wang 2006; Koter et al. 2015; Wang et al. 2016; Chen et al. 2023). The biological method is the most economical and effective approach for nitrate removal, mainly through denitrification, i.e., using specific enzymes in the microorganism to reduce nitrate. However, the composition of sewage wastewater varies significantly, which makes it challenging to find the appropriate strains and greatly affects the treatment results. Moreover, the biological method is a time-consuming process, which is often accompanied by the generation of secondary pollutants that are costly to treat (Ines et al. 1998; Ovez et al. 2006; Ghafari et al. 2008; Liang et al. 2021a, b).

Chemical reduction is a new class of NO<sub>3</sub><sup>-</sup> treatment technology developed in recent years, which reduces nitrate in water to non-toxic nitrogen (N<sub>2</sub>) or ammonia (NH<sub>3</sub>) of high economic value. Owing to the advantages of simple operation, high efficiency, and stability, electrocatalytic nitrate reduction has been extensively studied in

the water treatment field (Katsounaros et al. 2008). The development of high-performance cathode is the key to electrocatalytic nitrate reduction technology. The desirable cathode should have good stability, high conductivity and selectivity. To achieve desired activity and selectivity, common strategies including tuning the crystal structure, particle size, and geometry of the catalyst have been explored. The supporting materials also significantly affect the performance of the catalysts (Chen et al. 2021a, 2022a, b; Jin et al. 2022a). Previous researches have demonstrated the importance of suitable carriers in the preparation of high-efficiency catalyst, and biochar, metal oxide or metal hydroxide are considered as effective catalyst carriers for chemical reduction of nitrate (Qiu et al. 2015, 2021, 2022; Vilé et al. 2015; Yang et al. 2015; Chen et al. 2022a, b). Uniformly dispersed Pd–Cu bimetal catalysts were prepared through using TiO<sub>2</sub> nanofiber (Pd–Cu/TiO<sub>2</sub>) as a carrier, and the Pd–Cu/TiO<sub>2</sub> catalyst showed higher nitrate removal efficiency, N<sub>2</sub> selectivity, and faster removal kinetics, achieving nearly 100% conversion of NO<sub>3</sub><sup>−</sup> to harmless gas (Wang et al. 2017).

In recent years, due to its higher surface area and pore structure, as well as renewable characteristics, biochar has a wide range of applications in the fields of environmental protection, medicine, and food (Panee et al. 2015; Nirmala et al. 2018; Kumar et al. 2019; Liang et al. 2021a, b; Silva et al. 2021; Thotagamuge et al. 2021; Wei et al. 2022). Biochar presented the significant application potential in synthesis of BC and BC-based materials. At present, there are few studies on moso bamboo biochar as a metal catalyst carrier. Ho et al. (2019) prepared a high-performance carbon-catalyst for peroxydisulfate (PDS) activation based on C-phycoerythrin extracted (C-CP) *Spirulina*, which showed good oxidation degradation efficiency for various water micropollutants. Previous study has shown that bamboo sawdust could be used to prepare Fe–N biochar catalyst, which could effectively activate persulfate with good stability and high selectivity (Xu et al. 2020a, b). Liu et al. (2022) prepared an electrocatalyst by anchoring single atom Ru on Cu nanowires grown on three-dimensional Cu foam (Ru–Cu NW/CF) to remove NO<sub>3</sub><sup>−</sup> and the removal rate could reach about 94.1%. Jin et al. (2022c) constructed functionalized porous nanoscale Fe<sub>3</sub>O<sub>4</sub> particles supported biochar from peanut shell to remove Pb(II) ions from aqueous solution, showing that the maximum adsorption amount of Pb(II) could reach up to 188.68 mg g<sup>−1</sup>. A coconut shell biochar was applied as a support to construct a biochar-based composite (Ti<sub>3</sub>C<sub>2</sub>Tx@biochar-PDA/PEI) for the removal of U(VI) and Cs(I), and the results showed that the maximum adsorption capacity of U(VI) and Cs(I) were 239.7 and 40.3 mg g<sup>−1</sup>, respectively (Liu et al. 2023). Qiao et al. (2011) proposed the concept of single-atom

catalysts (SACs) to improve the efficiency of atom utilization and enhance the performance of the catalyst to a greater extent. For SACs, the active metals are supported on the carrier surface as single atoms and dispersed uniformly. They have great potential in bridging the gap between heterogeneous and homogeneous catalysts (Chen et al. a, 2018b; Qiao et al. 2011; Lang et al. 2016; Sun et al. 2022; Jin et al. 2022b). The effective steric isolation of metal active sites can suppress the side reactions that occur on aggregated metal active sites, thus improving catalytic selectivity (Li et al. 2020). The development and design of SACs can rationalize the use of metals and boost atomic economy by promoting atomic utilization efficiency. It has been proved that various catalytic reactions could be enhanced by the unique electronic structure and unsaturated coordination in SACs (Weon et al. 2020; Liu et al. 2016; Guo et al. 2014). SACs have great potential for improved selectivity due to their unique geometric structure of active sites, spatial and electronic interactions compared with homogeneous catalyst analogs (Liu et al. 2017; Choi et al. 2016; Yang et al. 2016; Chen et al. 2021b).

In this work, Pd–Cu biochar-based single-atoms catalysts (Pd–Cu–N–BC SACs) were synthesized by introducing Pd and Cu onto the nitrogen-doped bamboo biochar by an impregnation-calcination-reduction method. The electrocatalytic removal of nitrate by Pd–Cu–N–BC was evaluated in a 3D electrocatalytic reduction system. The catalytic activity, selectivity and reusability of the catalyst as well as the mechanism of the collaborative catalytic reduction of NO<sub>3</sub><sup>−</sup> by Pd–Cu–N–BC were systematically studied. Overall, this research highlights the great potential of Pd–Cu–N–BC SACs supported on N-BC and provides valuable insights for designing the highly efficient biochar-based electrocatalysts for environmental applications.

## 2 Experimental section

### 2.1 Synthesis and characterizations of Pd–Cu–N–BC SACs

The bamboo blocks (10 × 10 × 3 mm<sup>3</sup>) were activated with 2% NaOH solution at 80 °C for 3.5 h, and then washed and dried at 60 °C for 6 h. The dried bamboo block and nitrogen source precursor (dicyandiamide, dicy) were placed in 60 mL of deionized water at a mass ratio of 1:4, and stirred at 80 °C until dry. Then, the mixture was calcined in a tubular furnace at 800 °C for 1 h in a N<sub>2</sub> atmosphere. After cooling down to room temperature, the product was grinded to yield N-BC powder.

PdCl<sub>2</sub> and CuCl<sub>2</sub> were used as precursors of Pd and Cu, and the PdCl<sub>2</sub> and CuCl<sub>2</sub> were completely dissolved in 50 mL of 3% PEG solution to obtain a homogeneous mixed solution. Then, 0.5 g N-doped biochar was added to the mixed solution and subjected to ultrasonication

for 30 min. Afterwards, 0.01 M  $\text{NaBH}_4$  was added under stirring at 130 rpm for reduction of Pd and Cu. After filtrating, washing, and freeze-drying, the biochar-based Pd–Cu single-atom catalyst with N doping was obtained, which was denoted as Pd–Cu–N–BC.

Field emission scanning electron microscope (FESEM, JSM-7900F, Japan), transmission electron microscope (TEM, JEM-2010HR, Japan), and high angle annular dark field scanning transmission electron microscope (HAADF-STEM, FEI Themis, USA) were employed to characterize the morphology of the Pd–Cu supported catalysts. Powder X-ray diffraction pattern (XRD) and X-ray photoelectron spectrum (XPS) of the catalyst were collected on an X-ray diffractometer (X'Pert3 Powder, Netherlands) and a Kratos Axis Supra system (XPS, Thermo Fisher, USA), respectively. The electrochemical detection was carried out with an electrochemical workstation (Gamry, Interface1010E, USA).

## 2.2 Catalytic experiment

The electrocatalytic reduction of  $\text{NO}_3\text{-N}$  was carried out in a plexiglass tank ( $10 \times 5 \times 6 \text{ cm}^3$ ) as shown in Fig. 1. A homogeneous cation exchange membrane separated the reactor into cathode and anode chamber, and Pd–Cu–N–BC particles acted as three-dimensional particle electrodes in the cathode chamber to enhance the catalytic reduction reaction. Titanium ruthenium

plates with an area of  $4.5 \times 3.5 \text{ cm}^2$  were used as anode and current collector of the cathode, respectively. A pre-set concentration of  $\text{NO}_3\text{-N}$  solution was added to the cathode chamber with sodium sulfate as supporting electrolyte, and same concentration of sodium sulfate solution as the cathode chamber was added to the anode chamber. The cathode chamber was continuously stirred during the reaction. Solution was sampled at pre-determined intervals and filtered to analyze the removal rate of  $\text{NO}_3\text{-N}$  and the production of  $\text{NO}_2^-$ ,  $\text{NH}_4^+$ , and  $\text{N}_2$ . All experiments were performed in triplicate.

## 2.3 Analysis methods

The detection and quantification of nitrate and its products were performed using an ultraviolet and visible spectrophotometer according to national standards (HJ T 346-2007, GB7493-1987 and HJ 535-2009). In this work, the other intermediates ( $\text{N}_2\text{O}$ ,  $\text{NO}$ , etc.) were extremely unstable in the electrolytic reduction process, and were easily degraded into  $\text{NO}_2^-$  and  $\text{N}_2$  in the system. The dissolution amount in aqueous solution was very low, so the production amount of these types of intermediates could be ignored.

The removal rate ( $\eta$ ) of  $\text{NO}_3^-$  could be calculated by the Eq. 1:

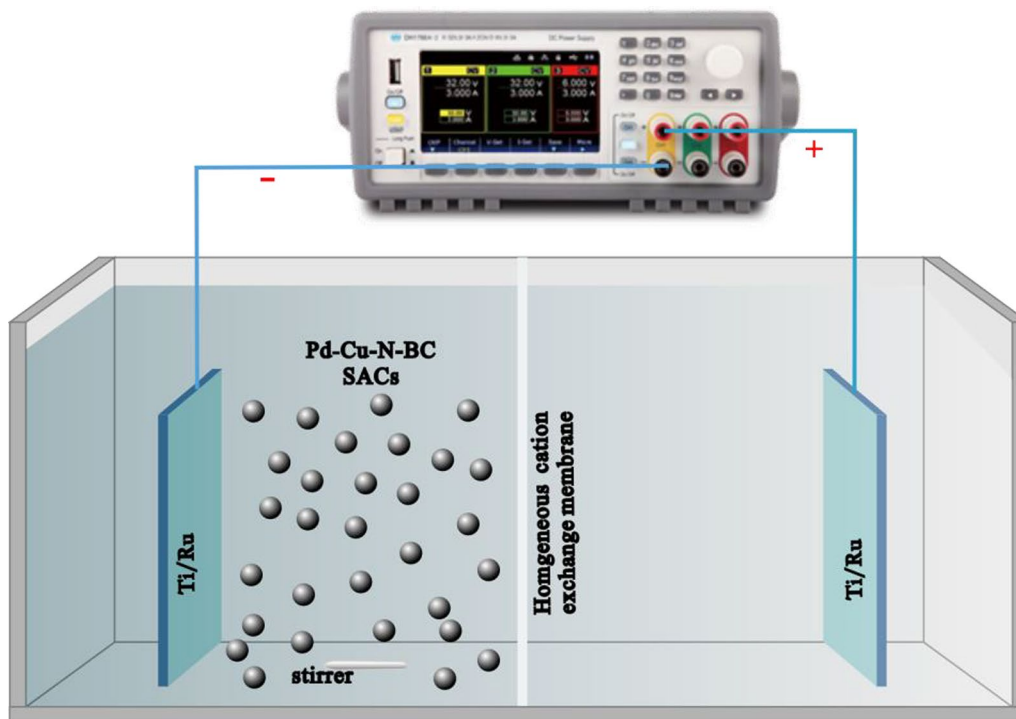


**Fig. 1** Schematic diagram of the electrocatalytic reduction reactor

$$\eta = \left(1 - \frac{[\text{NO}_3^- - \text{N}]_t}{[\text{NO}_3^- - \text{N}]_0}\right) \times 100\% \quad (1)$$

where  $[\text{NO}_3^- - \text{N}]_0$  represents the initial concentration of  $\text{NO}_3^- - \text{N}$  and  $[\text{NO}_3^- - \text{N}]_t$  is the concentration of  $\text{NO}_3^- - \text{N}$  at time  $t$  ( $\text{mg L}^{-1}$ ). The generation ratio of various products can be calculated according to the following Eqs. 2, 3, 4 (Gao et al. 2019).

$$S(\text{NO}_2^- - \text{N}) = \frac{[\text{NO}_2^- - \text{N}]_t}{[\text{NO}_3^- - \text{N}]_0 - [\text{NO}_2^- - \text{N}]_t} \times 100\% \quad (2)$$

$$S(\text{NH}_4^+ - \text{N}) = \frac{[\text{NH}_4^+ - \text{N}]_t}{[\text{NO}_3^- - \text{N}]_0 - [\text{NO}_2^- - \text{N}]_t} \times 100\% \quad (3)$$

$$\text{GR}(\text{N}_2) = \frac{[\text{NO}_3^- - \text{N}]_0 - [\text{NO}_3^- - \text{N}]_t - [\text{NO}_2^- - \text{N}]_t - [\text{NH}_4^+ - \text{N}]_t}{[\text{NO}_3^- - \text{N}]_0} \times 100\% \quad (4)$$

where  $S$  represents the ratio of products, and  $[\text{NO}_2^- - \text{N}]_t$  and  $[\text{NH}_4^+ - \text{N}]_t$  are the concentrations of  $\text{NO}_2^- - \text{N}$  and  $\text{NH}_4^+ - \text{N}$  at time  $t$ . The catalytic activity of catalyst was calculated via the Eq. 5 (Zhang et al. 2016):

$$A_{\text{mass}} = \frac{(C_{t_1} - C_{t_2})}{w_{\text{cat}} \times (t_1 - t_2)} \quad (5)$$

where  $A_{\text{mass}}$  denotes the amount of catalytic reduction of substrate per unit mass catalyst in one minute ( $\text{mg}(\text{g}_{\text{cat}} \text{min})^{-1}$ ),  $w_{\text{cat}}$  is the dose of catalyst ( $\text{g L}^{-1}$ ), and  $C_{t_1}$  and  $C_{t_2}$  are the concentration of substrates at time  $t_1$  and  $t_2$  ( $\text{mg L}^{-1}$ ), respectively.

### 3 Results and discussion

#### 3.1 Catalyst characterization

The SEM images of pristine biochar (BC) and N-BC prepared at 800 °C are showed in Fig. 2a, b. It can be seen that BC exhibited a honeycomb-like porous structure, which is beneficial for mass transfer and provided abundant loading space for Cu and Pd metals. In contrast, N-BC prepared at 800 °C presented a very distinct morphology of stacked layers and wrinkled sheets, which may be resulted from the incorporation of nitrogen atoms into the graphitic carbon lattice to form a large number of defects (Xu et al. 2020b). The TEM and EDX images (Fig. 2c, d) show that Pd and Cu metal atoms were uniformly dispersed on the N-BC support. The average size of the Pd or Cu nanoparticles was about 5.84 nm by HRTEM images, which also displayed the lattice fringes of the Pd and Cu particles. The d-spacings of

Pd and Cu nanoparticles on N-BC were about 0.226 nm and 0.210 nm corresponding to the (111) facet of Pd and Cu (Fig. 2e), respectively. In the HAADF image (Fig. 2f), many bright dots with atomic size and a few clusters were observed, indicating that Pd and Cu mainly existed in the form of individual atoms, which were stabilized by carbon or nitrogen.

The normalized XANES spectra at Cu and Pd K-edge of Pd-Cu-N-BC are showed in Fig. 2g, h. The results represented the absorption edge of the XANES spectrum of the Pd-Cu-N-BC shifted toward higher energies and nearly coincided with the spectra of the metal oxide specimens (CuO and PdO) compared with those of the standard samples of Pd foil, Cu foil, PdO, and CuO. This phenomenon revealed that Pd and Cu species in the catalyst existed as single atoms, and were gradually

oxidized to form their metal oxides after being stored in the atmosphere at room temperature for some time. Comparing the R-space EXAFS of a series of Cu samples (Fig. 2i, j), it was found that Cu foil showed a clear characteristic peak belonging to the EXAFS of the Cu-Cu bond at about 2.5 Å. And Pd foil also displayed a clear characteristic peak belonging to the EXAFS of Pd-Pd bond at about 2.5 Å. However, for the Pd-Cu-N-BC catalyst, the characteristic EXAFS peaks attributed to Cu-N and Pd-N appeared only at 1.5 Å without any contribution from the Cu-Cu and Pd-Pd bonds. In the previous HAADF-STEM characterization results, it has been proved the existence of scattered single distributed metal atoms of Pd and Cu in Pd-Cu-N-BC SACs. Herein, the EXAFS results demonstrated that the Pd and Cu metal atoms were anchored in the biochar lattice successfully, which was consistent with previous studies. The wavelet transform contours of Pd-Cu-N-BC, the standard samples of Cu and Pd foils, CuO and PdO are presented in Fig. 2k-o. It can be seen from the figure that homogeneously dispersed metal atoms existed in the structure of the Pd-Cu-N-BC catalyst. Moreover, only Pd-N and Cu-N bonds existed, while no chemical bonds related to Pd/Cu nanoparticles or Pd/Cu metal clusters emerged.

To further verify the atomic structures of Pd and Cu active sites in the Pd-Cu-N-BC, X-ray photoelectron spectroscopy (XPS) was applied to characterize the electronic structure of catalyst (Fig. 3a-d). According to the XPS result, the binding energy of Cu 2p 932.59 eV, which was 0.19 eV higher than that of Cu<sup>0</sup> foil (932.4 eV), but 1.01 eV lower than that of CuO (933.6 eV). It revealed that the valence of Cu in Pd-Cu-N-BC catalyst was between 0

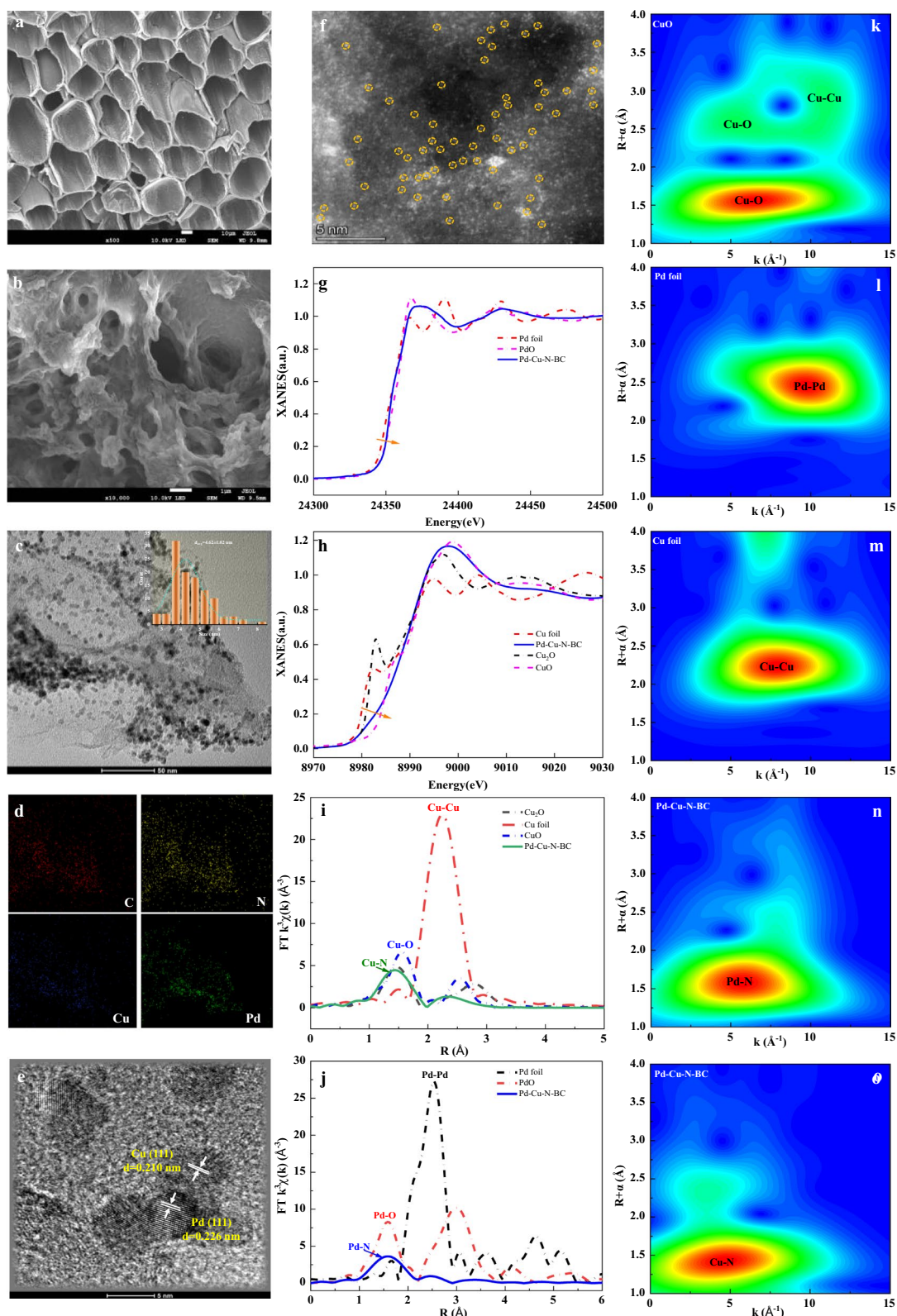


**Fig. 2** Morphological characterization of catalysts. **a, b** SEM of pristine BC and N-BC at 800 °C; **c–e** TEM, TEM–EDX and lattice spacing of Pd–Cu–N-BC; **f** HAADF-STEM of Pd–Cu–N-BC (SACs: yellow circles); **g, h** Normalized XANES spectra at Cu and Pd K-edge of Pd–Cu–N-BC; **i, j** Fourier transformed magnitudes of the experimental Pd or Cu K-edge for Pd foil, PdO, Cu foil and CuO; **k–o** EXAFS wavelet transform contour for the  $k^3\chi(k)$  function of CuO, Pd foil, Cu foil, and Pd–Cu–N-BC

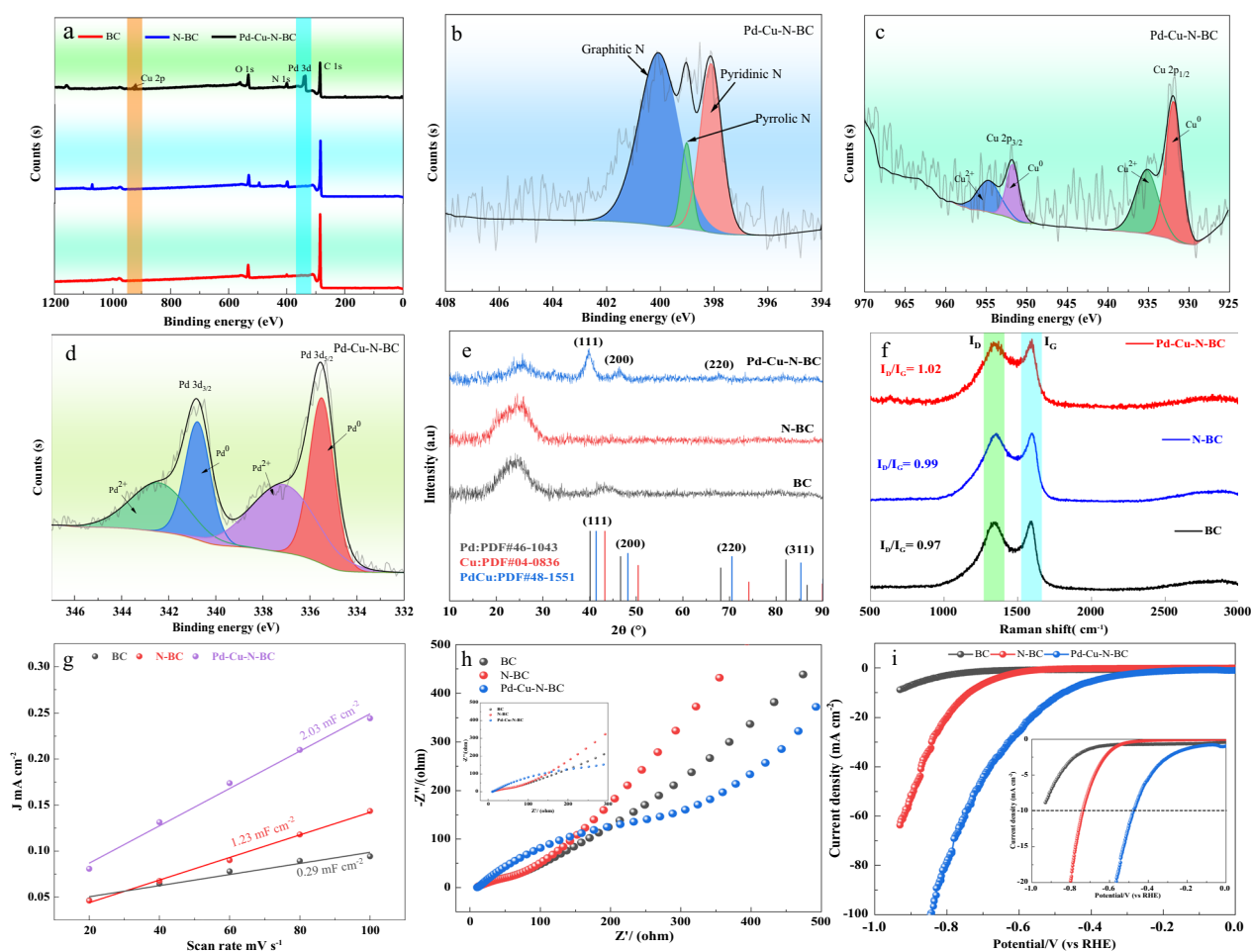


**Fig. 3** a–d XPS spectra of BC, N-BC, and Pd–Cu–N-BC; e XRD spectra of BC, N-BC, and Pd–Cu–N-BC; f Raman spectra of BC, N-BC, and Pd–Cu–N-BC; g–i ECSA, EIS and LSV spectra of BC, N-BC, and Pd–Cu–N-BC

and +2 (Zhao et al. 2022). The XPS results demonstrated that N atoms had been successfully doped into the biochar lattice. The high-resolution N 1s XPS spectrum of the catalyst showed three peaks with binding energies at 398.08, 399.07, and 400.2 eV, which are assigned to pyridinic N, pyrrolic N, and graphitic N, respectively (Duan et al. 2015; Guo et al. 2018; Xu et al. 2020b), and the percentages were 36.25%, 24.40% and 39.35% respectively in this study. Both graphitic and pyridinic N have remarkable redox reaction potential, which favors the generation of hydrogen radicals. The high-resolution XPS spectra of Pd 3d and Cu 2p revealed the presence of Pd and Cu atoms or clusters, which confirmed that metal atoms were loaded and anchored by a nitrogen atom in the biochar lattice.

XRD patterns of Pd–Cu–N-BC, N-BC, and BC are shown in Fig. 3e. Two diffraction peaks at 23° and 43.5° were presented in the XRD pattern of BC, corresponding to the (002) and (100) planes of amorphous and

crystalline carbon, respectively (Li et al. 2019; Xu et al. 2020b). It is obvious that nitrogen doping makes the peak at 23° stronger due to the introduction of nitrogen into the lattice of biochar (Chen et al. a, 2018b). For the Pd–Cu–N-BC, the characteristic diffraction peaks at 40°, 47°, 70.3°, and 85.5° match well with (111), (200), (220), and (311) crystal facets of Pd (PDF#46-1043, PDF#48-1551). However, no appreciable diffraction peaks related to Cu can be distinguished, which may be attributed to the well dispersion of Cu single atoms in the catalyst. The results also proved that Pd and Cu atoms had been successfully supported in the lattice of the prepared catalyst. The Raman spectra of BC, N-BC, and Pd–Cu–N-BC are given in Fig. 3f. Generally, the Raman spectra have two characteristic peaks around 1344 cm<sup>-1</sup> and 1579 cm<sup>-1</sup> belonging to disordered carbon (D band) and graphitic carbon (G band), respectively. It is evident that the intensity ratio of the D band to G band ( $I_D/I_G=1.02$ ) of Pd–Cu–N-BC catalyst is higher than that of BC and N-BC, suggesting a

higher level of defects. The level of defect in the catalyst structure significantly affects the adsorption of hydrogen and the transfer of free  $\pi$ -electrons to active hydrogen to generate free radicals (Duan et al. 2015; Xu et al. 2020b). Nitrogen doping can increase the defects in the lattices of biochar, which is beneficial for anchoring and dispersion of metal atoms on the surface of biochar.

Electrochemical measurements were performed to explore the electrochemical property of particle electrodes and the influence of nitrogen doping. The basic characteristics of the particle electrodes were analyzed by steady-state polarization. The electrochemical active surface area (ECSA) was obtained by doing cyclic voltammetry (CV) measurements at different scan rates in the non-Faradic region. As shown in Fig. 3g, the ECSA of Pd-Cu-N-BC ( $2.03 \text{ mF cm}^{-2}$ ) was larger than that of BC ( $0.29 \text{ mF cm}^{-2}$ ) and N-BC ( $1.23 \text{ mF cm}^{-2}$ ), suggesting a better catalytic performance of Pd-Cu-N-BC for  $\text{NO}_3^-$ -N electrocatalytic reduction.

The resistance properties of particle electrodes were also analyzed by the transient-state electrochemical impedance spectroscopy (EIS). The Nyquist plots of pristine biochar, nitrogen biochar, and Pd-Cu-N-BC are shown in Fig. 3h. The plots of catalysts displayed semi-circles of different radii in the high-frequency region, symbolizing different electrical conductivity of their charge-transfer resistance ( $R_{ct}$ ) (Zhang et al. 2019; Li et al. 2022a, b). The lower  $R_{ct}$  of Pd-Cu-N-BC was ascribed to its higher conductivity and lower electron transfer resistance. The results also proved that the electronic structure of Pd-Cu-N-BC was efficiently optimized through nitrogen doping. The catalytic performance of Pd-Cu-N-BC could be enhanced by modulation the Pd and Cu coordination through nitrogen doping.

Linear sweep voltammetry (LSV) measurements were performed in 1.0 M KOH solution and the results of each material are shown in Fig. 3i. There was obvious difference in the potential value required (overpotential) for the reference current density ( $\eta_{10}$ ,  $10 \text{ mA cm}^{-2}$ ) of the catalysts, which reflect the difficulty of the hydrogen evolution reaction (HER). The overpotential of Pd-Cu-N-BC ( $-0.47 \text{ V}$ ) was lower than that of BC (no detected) and N-BC ( $-0.72 \text{ V}$ ), confirming that HER was more likely to occur in Pd-Cu-N-BC system to generate hydrogen radical ( $\text{H}^*$ ) for  $\text{NO}_3^-$  reduction.

## 3.2 Catalytic performance of the Pd-Cu-N-BC

### 3.2.1 Precursors concentration

The concentration of precursors plays an important role in determining the catalytic performance of the catalysts and the Pd and Cu metal loading ratio is given in Table 1. The electrocatalytic reduction of  $\text{NO}_3^-$ -N in water by Pd-Cu-N-BC is shown in Fig. 4a-c. The results indicated that

**Table 1** Metal load of impregnated supported catalyst at different precursor concentrations

Type of catalyst	Metal loading (wt%)	
	Pd	Cu
$\text{Pd}_{0.30}\text{Cu}_{0.075}\text{-N-BC}$	2.48	0.78
$\text{Pd}_{0.60}\text{Cu}_{0.15}\text{-N-BC}$	4.89	1.37
$\text{Pd}_{0.80}\text{Cu}_{0.20}\text{-N-BC}$	5.59	1.33
$\text{Pd}_{1.00}\text{Cu}_{0.25}\text{-N-BC}$	8.71	5.33

the electro-catalytic removal rate of  $\text{NO}_3^-$ -N increased with the increase of the concentration of  $\text{Pd}^{2+}$ . When the concentrations of  $\text{Pd}^{2+}$  and  $\text{Cu}^{2+}$  were  $0.80 \text{ g L}^{-1}$  and  $0.20 \text{ g L}^{-1}$  in the precursor solution, the  $\text{NO}_3^-$ -N removal was 100%. When the concentration of  $\text{Pd}^{2+}$  was further increased to  $1.00 \text{ g L}^{-1}$ , the selectivity of  $\text{N}_2$  decreased significantly (Fig. 4d). The decrease in  $\text{N}_2$  generation may be related to the decrease in the number of SACs in the catalyst, as the active sites are more likely to be present in the form of nanoparticles at higher concentrations. Therefore, under the optimal concentration of  $\text{Pd}^{2+}$  of  $0.80 \text{ g L}^{-1}$ , Pd and Cu atoms could be loaded successfully and dispersed on the surface of the biochar lattice uniformly, and the kinetic constant value of catalytic performance was 0.0147 through the first order reaction kinetics simulation.

### 3.2.2 Initial $\text{NO}_3^-$ -N concentration

Using the titanium-ruthenium plate as anode and current collector for cathode in the reactor, electrocatalytic reduction experiments were carried out with different initial concentrations of nitrate solutions at pH 7.0. The concentration of  $\text{Na}_2\text{SO}_4$  electrolyte solution was  $0.20 \text{ g L}^{-1}$  and current density was  $3.17 \text{ mA cm}^{-2}$ . The experimental results are presented in Fig. 5a-c. The results showed that the removal rate of  $\text{NO}_3^-$ -N in the solution decreased with the increase of the initial concentration of  $\text{NO}_3^-$ . And with the increase of the initial concentration of  $\text{NO}_3^-$ -N, the generation of  $\text{N}_2$  increased at first and then decreased (Fig. 5d). Considering the nitrate removal rate and  $\text{N}_2$  generation together, Pd-Cu-N-BC had a high catalytic efficiency when the  $\text{NO}_3^-$ -N initial concentration was  $100 \text{ mg L}^{-1}$ , and the kinetic constant value was 0.0205 through the first order reaction kinetics.

### 3.2.3 Current density

Current density is considered to be one of significant factors affecting the reaction rate. Therefore, the effect of current density on the electrocatalytic reduction of nitrate was investigated in this work. The removal of  $\text{NO}_3^-$ -N, and the generation of  $\text{NO}_2^-$  and  $\text{NH}_4^+$  under different current densities are shown in Fig. 6a-d. The



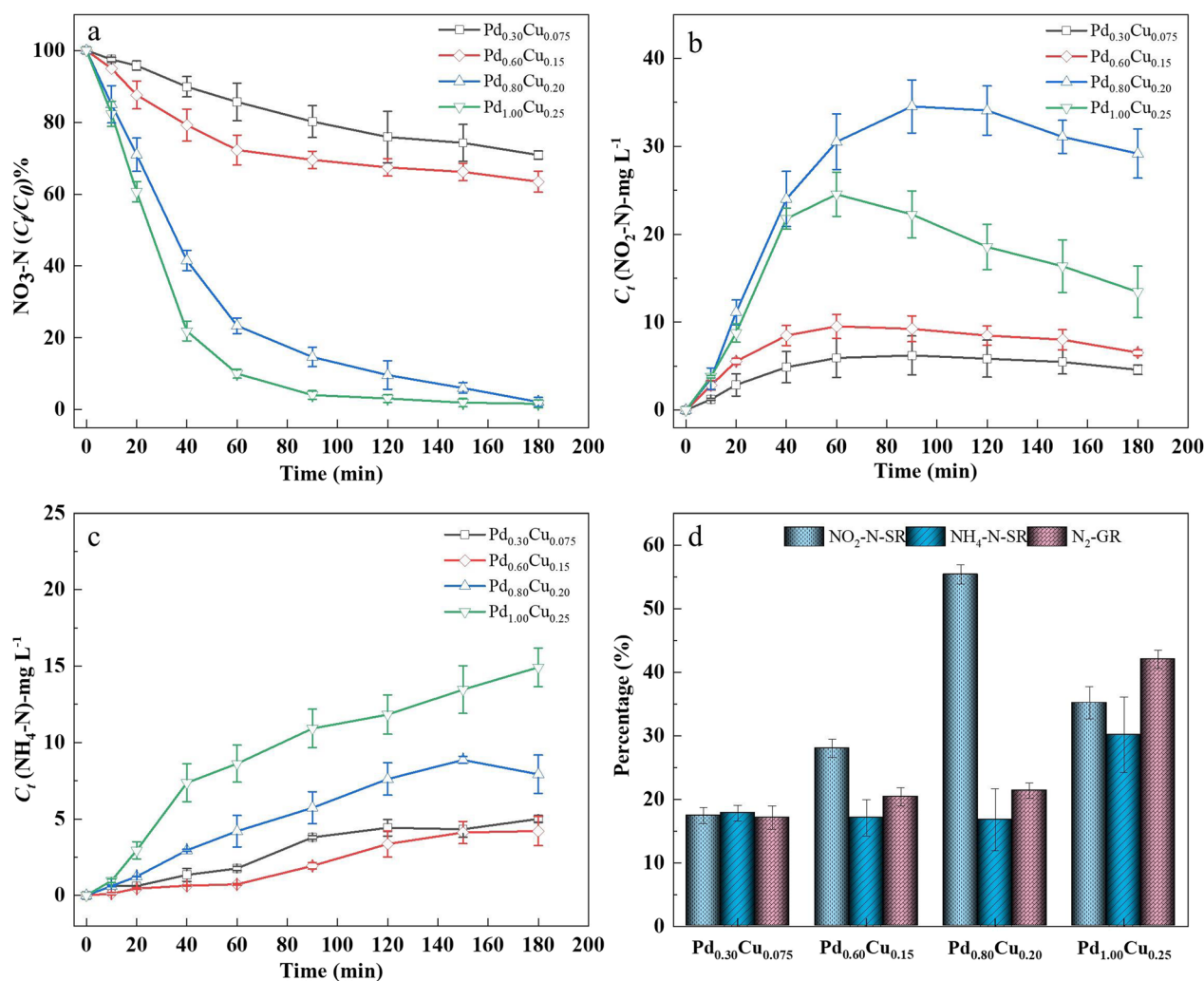


**Fig. 4** Effect of electrocatalytic reduction of nitrate at different concentrations of precursors (**a**: the removal of NO<sub>3</sub>-N; **b-c**: the generation of NO<sub>2</sub>-N and NH<sub>4</sub>-N; **d**: the selectivity rate of NO<sub>2</sub>-N, NH<sub>4</sub>-N and the generation rate of N<sub>2</sub>)

results indicated that the removal rate of NO<sub>3</sub>-N could reach about 95% at 180 min when the current density was increased from 1.90 to 8.25 mA cm<sup>-2</sup>. Additionally, the generation of N<sub>2</sub> increased with the current density increased to 6.98 mA cm<sup>-2</sup>, and the kinetic rate constant was 0.0186. Further increase in current density led to the decrease in both NO<sub>3</sub><sup>-</sup> removal rate and N<sub>2</sub> generation. Excessive current density leads to high energy consumption, which will lead to higher treatment cost and is contrary to green chemistry.

### 3.2.4 pH

The pH value is also an important parameter to regulate the NO<sub>3</sub>-N removal in the aqueous phase. Figure 7a shows that the removal rate of NO<sub>3</sub>-N showed a decreasing trend with the increase of pH from 3.0 to

9.0. Moreover, both the removal rate of NO<sub>3</sub>-N and the generation of N<sub>2</sub> could reach the peak at pH=7 (Fig. 7d). The results revealed that the change of pH could affect the reduction of NO<sub>3</sub>-N and the generation of N<sub>2</sub>. With the increase of pH value, the concentration of OH<sup>-</sup> ions increased, and OH<sup>-</sup> ions occupied the surface of the metal catalyst. Consequently, NO<sub>3</sub><sup>-</sup> and NO<sub>2</sub><sup>-</sup> adsorbed on the surface of the metal decreased, and the amount of hydrogen produced by electrolysis adsorbed on the metal surface was also decreased (Fig. 7b). Correspondingly, the reduction rate slowed down, and the probability of ammonia (NH<sub>4</sub><sup>+</sup>) generation also increased (Fig. 7c). Herein, an acidic or alkaline water environment is not favorable for the removal of NO<sub>3</sub>-N from water, while neutral water environment is favorable for the harmless treatment of nitrate by

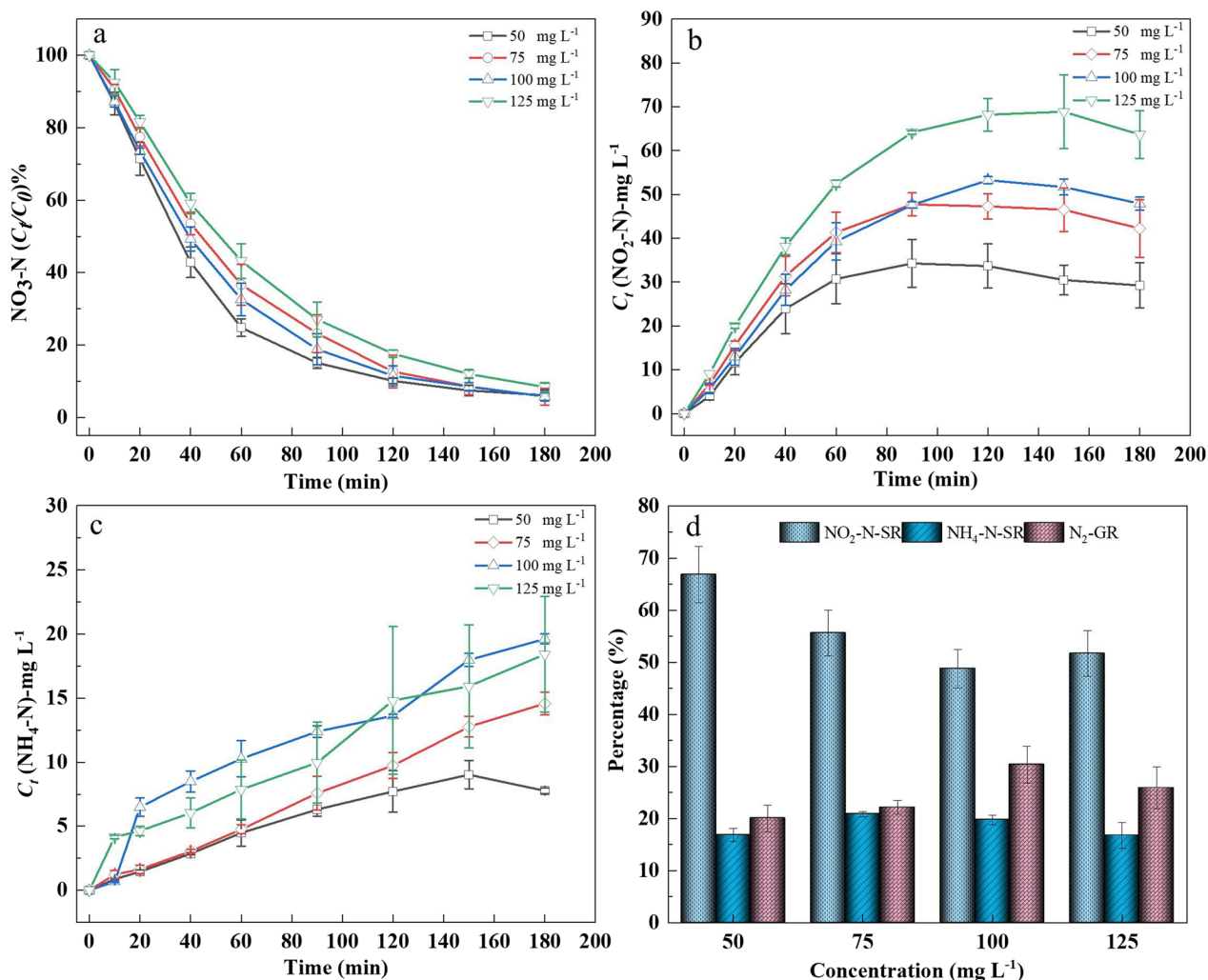
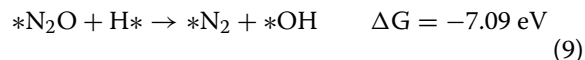
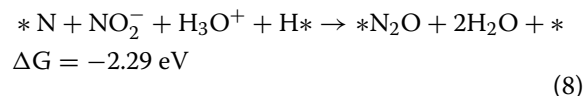
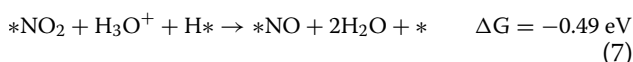
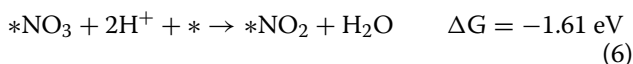


**Fig. 5** Effect of electrocatalytic reduction of nitrate at a different initial concentration of nitrate (**a**: the removal of NO<sub>3</sub>-N; **b-c**: the generation of NO<sub>2</sub>-N and NH<sub>4</sub>-N; **d**: the selectivity rate of NO<sub>2</sub>-N, NH<sub>4</sub>-N and the generation rate of N<sub>2</sub>)

Pd–Cu–N–BC and the kinetic constant value was 0.0186 for catalytic performance.

### 3.3 Role of H\*

In order to further understand the important contribution of H\* versus direct cathodic reduction in reaction system, the different concentrations of TBA (tert-butanol) were added to quench H\* in the experiments. H\* may be involved in indirect reduction and to the process reaction pathways are shown in Eqs. 6–9.



As shown in Fig. 8a, increasing the concentration of TBA in the electrolyte could lead to the decrease of the nitrate removal and N<sub>2</sub> generation. These results have shown the active role of H\* in the nitrate reduction process, corresponding to the previous research (Shin et al. 2014; Niu et al. 2020; Zheng et al. 2022). TBA can be used as a shielding agent to consume the H\* produced during the electroreduction reaction to form the inert 2-methyl-2-propanol free radicals, When the catalytic reduction reaction was carried out for 90 min, the inhibition effect of tert-butanol as the shielding agent of atomic

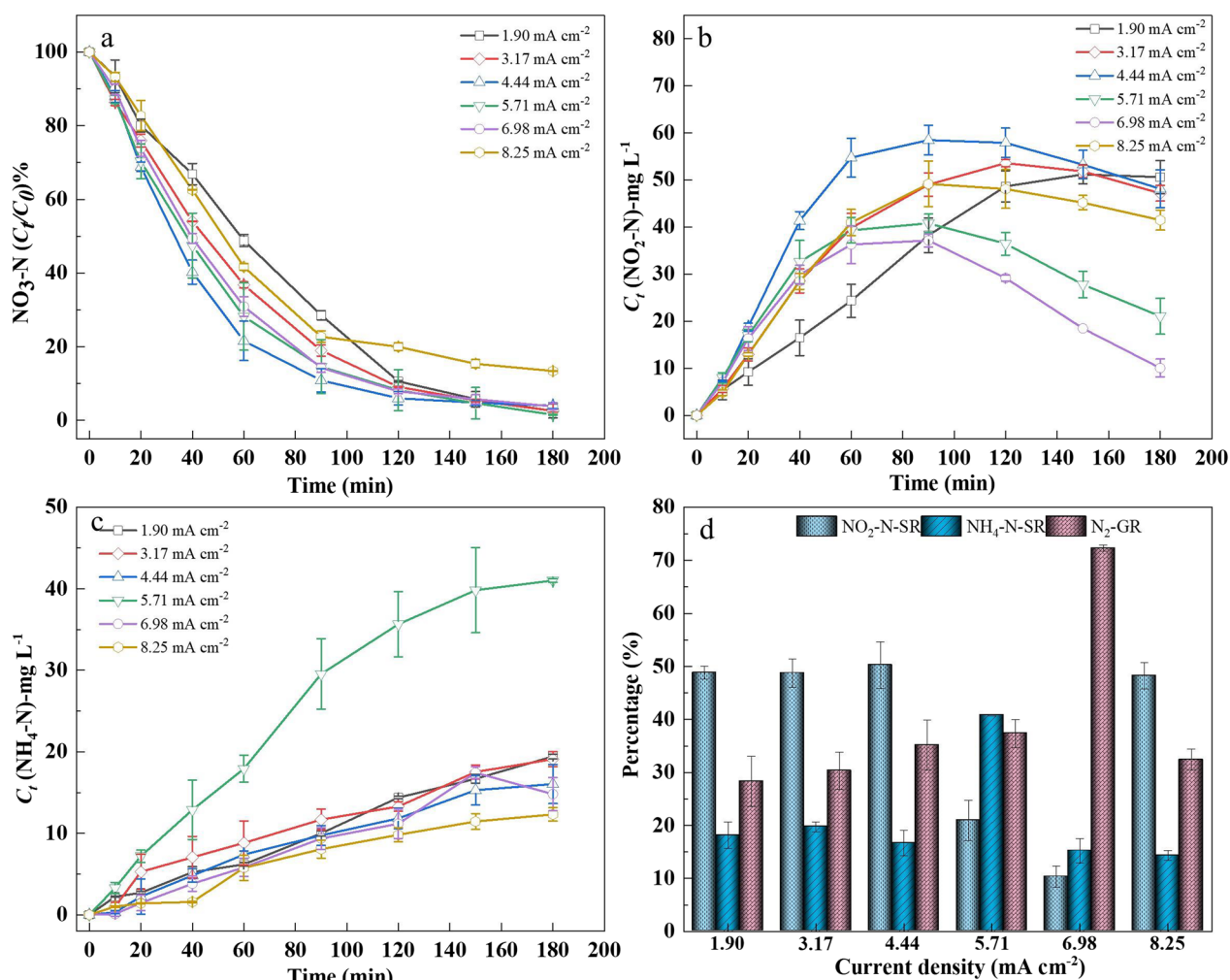


**Fig. 6** Effect of electrocatalytic reduction of nitrate at a different current density (**a**: the removal of NO<sub>3</sub>-N; **b-c**: the generation of NO<sub>2</sub>-N and NH<sub>4</sub>-N; **d**: the selectivity rate of NO<sub>2</sub>-N, NH<sub>4</sub>-N and the generation rate of N<sub>2</sub>)

hydrogen H<sup>\*</sup> was obvious. When no tert-butanol was added, the nitrate removal rate in the reaction system basically reached 100%, and the nitrogen generation rate was 72.32%. When 0.2 M, 0.5 M and 1.0 M TBA solutions were added, the removal rates of nitrate in the system decreased to 87%, 71% and 60%, respectively. The nitrogen generation rate also decreased significantly, which was 39%, 29% and 23%, respectively (Fig. 8b). When the concentration of TBA was 0.2 M, the removal rate of nitrate was reduced by about 33% after 90 min, which revealed that H<sup>\*</sup> played an important role in the nitrate reduction process.

### 3.4 Mechanistic studies by DFT of electrocatalysis

In order to understand the mechanism of electrocatalytic reduction of nitrate at the molecular level, the

relationship between the structure, Gibbs free energy, and catalytic performance of Pd-Cu-N-BC was explored by DFT calculations. Pd and Cu metal atoms were embedded in the N-doped biochar lattice, and coordinated with pyridine nitrogen in the structure of Pd-N<sub>4</sub> and Cu-N<sub>4</sub>, respectively. The results of geometric structure optimization showed that the Pd-Cu-N-BC maintained a relatively good planar relationship with N atoms as dopant, which facilitated the optimization of the intermediate state adsorption and promoted the hydrogen evolution performance of the catalyst (HER), resulting in a stable single-atom catalyst structure.

Previous reports have displayed theoretically based on DFT calculation that there are several conventional pathways for the nitrate reduction (Niu et al. 2020; Zhu et al. 2020; Daiyan et al. 2021; Zhao et al. 2022). Based on the existing researches, the possible pathways were given for

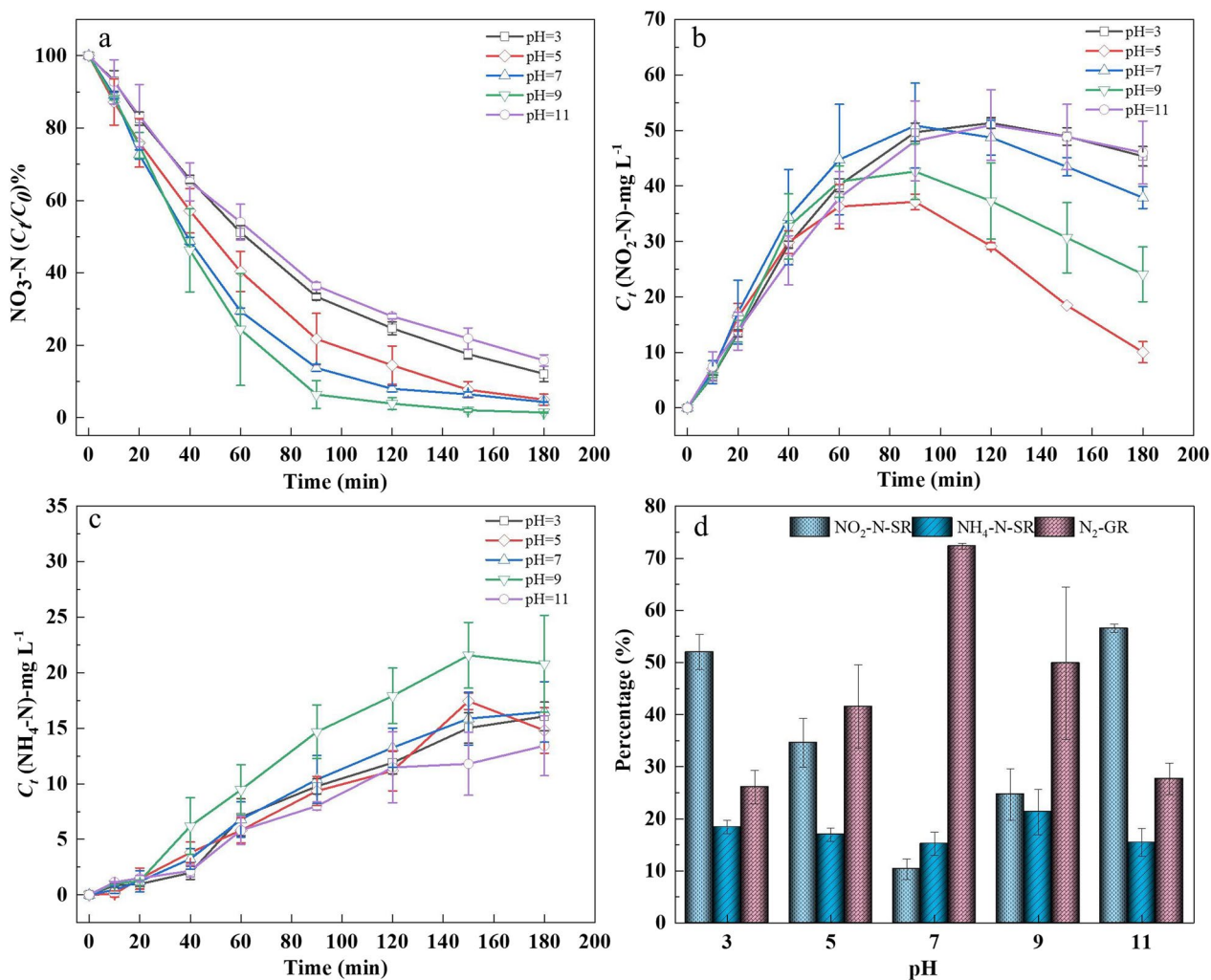


**Fig. 7** Effect of electrocatalytic reduction of nitrate at different pH values (a: the removal of NO<sub>3</sub>-N; b-c: the generation of NO<sub>2</sub>-N and NH<sub>4</sub>-N; d: the selectivity rate of NO<sub>2</sub>-N, NH<sub>4</sub>-N and the generation rate of N<sub>2</sub>)

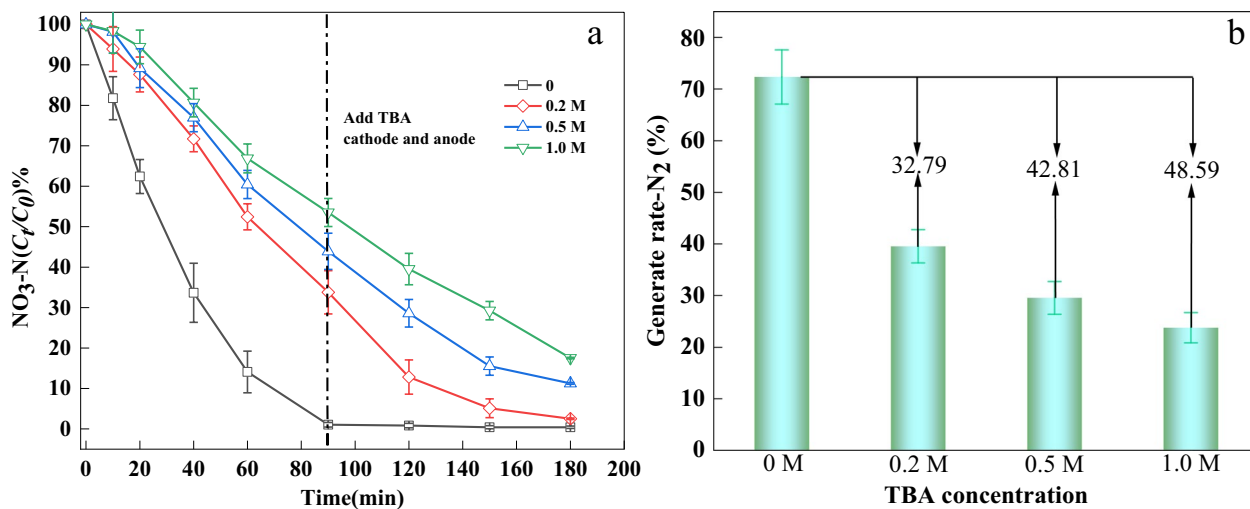
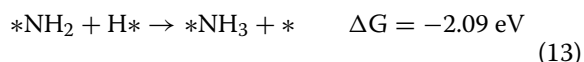
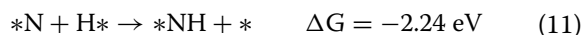
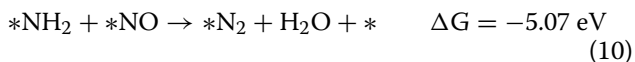


**Fig. 8** Effect of different concentrations of TBA on nitrate removal and N<sub>2</sub> generate rate in the reaction system (a: the removal of NO<sub>3</sub>-N after adding TBA in cathode and anode; b: the generation rate of N<sub>2</sub> after adding TBA in cathode and anode)

electrochemical reduction of nitrate to nitrogen driven by Pd–Cu–N-BC in this research (Eqs. 6–13).



The results of the intermediates and Gibbs free energy calculations under various reaction conditions are shown in Fig. 9. The calculations showed that Gibbs free energy of nitrate reduction was an overall negative value, corresponding to the previous reports (Daiyan et al. 2021; Xu et al. 2021).

Cu can be considered as the most effective metal for electrocatalytic reduction of  $NO_3^-$ –N (Dima et al. 2003; Casella et al. 2004; Pérez-Gallent et al. 2017), while Pd has been known to actively and selectively reduce  $NO_2^-$  to  $NH_4^+$  or  $N_2$  (Pintar et al. 2004; Souza-Garcia et al.

2012). During the electrocatalytic reduction, Pd and Cu metal sites served as the reactive sites for nitrate reduction. From the free energy diagram, the formed  $*NO_3^-$  could be reduced to  $*NO_2^-$  with energy change of 1.61 eV through an entirely exothermic process. Subsequently,  $*NO_2^-$  was transferred around the Pd atom to obtain  $2H^+$  to form  $*NO$ , and this energy change in the free energy profile was 0.49 eV for Pd–Cu–N-BC. There was no obvious energy barrier to the process from  $*NO_3^-$  to  $*NO$ . Following, the process from  $*NO$  to  $*N$  was an endothermic reaction accompanied with the free energy increased by 1.39 and 1.21 eV for the intermediate product  $*NOH$  and  $*N$ , respectively. Starting from this process, there are two sub-pathways for  $N_2$  formation (Fig. 9). H proton attacks the intermediate  $*N$  continuously in the cathode chamber, leading to the energy dropped by 2.29 and 8.89 eV for the formation of  $*N_2O$  and  $*N_2$  in the first sub-pathway, respectively. Meanwhile, in the other sub-pathway, the free energy of 9.31 eV is required during the process from  $*N$  to  $*N_2$ . Eventually, intermediate states could combine with each other

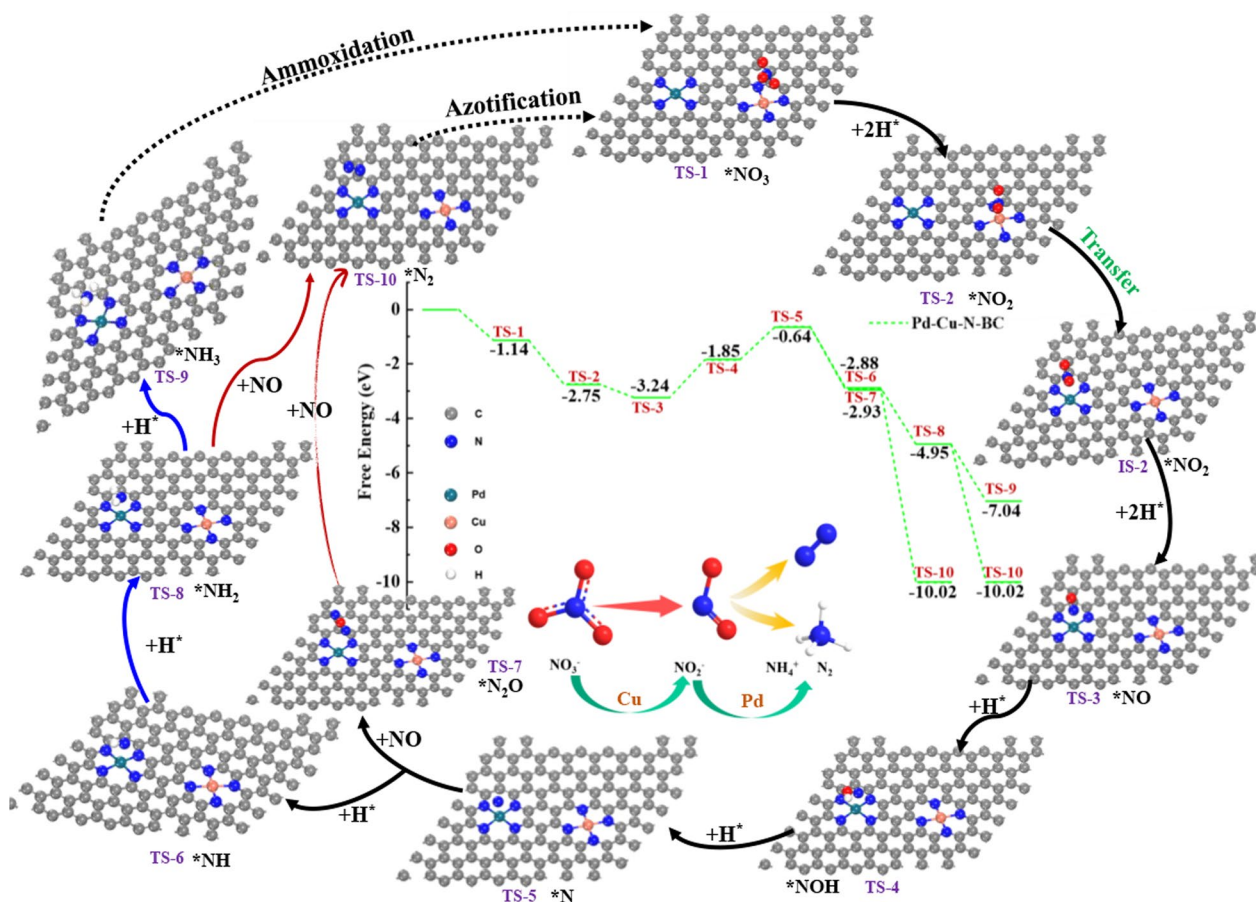


**Fig. 9** Mechanism of electrocatalytic reduction of nitrate on Pd–Cu–N-BC SACs

to form coupled  $N_2$  in electrocatalytic reduction system (Prüsse et al. 2000).

In the whole process of reduction, the end products were regulated by the Pd atom, depending on the adsorption energy of  $*NH$  bound to  $H^*$  or  $*N_2O$  bound to  $*NO$ . According to the reaction pathway, the active sites around the Pd atom would provide more energy for  $*N_2O$  to combine with  $*NO$  to generate  $N_2$ , which can easily escape from the chamber due to its inertness and poor solubility. Nitrogen doping could reasonably modulate the electronic structure of Pd and Cu sites in the catalysts at the atomic level and enhance electrocatalytic reduction of nitrate. Corresponding to experimental results, Pd and Cu metal atoms cooperated to complete the reduction of

nitrate and obtain a high selectivity of nitrogen (72.32%). Pd–Cu–N–BC achieved efficient electrocatalytic removal of nitrate with high  $N_2$  selectivity, which provided theoretical support and technical reference for the pollution prevention and control of nitrate in groundwater.

### 3.5 Reusability and stability of Pd–Cu–N–BC

Stability is the one of the important indicators to evaluate the practical application of the catalyst. The reusability and stability of Pd–Cu–N–BC were considered and explored in this work. In the experiments, the  $NO_3^-$ -N removal rate and mass-normalized catalytic activity ( $A_{mass}$ ) were assessed by cycle test. The results are shown in Fig. 10. After three cycles of catalytic reduction experiments, the removal rate of  $NO_3^-$  declined from 99.65% to 89.72%. Additionally, in the first cycle experiment, the catalytic activity of Pd–Cu–N–BC was  $0.6894 \text{ mg (g}_{cat} \text{ min)}^{-1}$  (Eq. 5). During the second and third cycles, the catalytic activity decreased to  $0.6643 \text{ mg (g}_{cat} \text{ min)}^{-1}$  and  $0.6282 \text{ mg (g}_{cat} \text{ min)}^{-1}$ , respectively, which decreased only by 3.6% and 8.9% compared to the first cycle. Moreover, the catalytic activity of the 3D SACs in this study was about 2.54 times higher than that reported by Wu et al. (2022). The comparison with other materials is listed in the Table 2, which indicates that the Pd–Cu–N–BC SACs possessed a great potential to reduce nitrate and harmless disposal. Therefore, the active components in the catalyst can maintain a high stability in the electrocatalytic reduction system and have high efficiency in the electrocatalytic removal of nitrate.

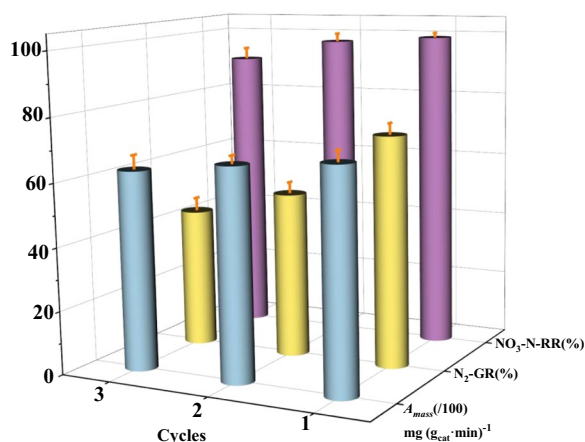


**Fig. 10**  $NO_3^-$ -N removal rate and mass-normalized catalytic activity in three cycles

**Table 2** The comparison of nitrate removal from water through the different materials

Material	Metal elements form	$NO_3^-$ -N removal (%)	$NH_4^-$ -N selectivity	$N_2$ -generation	Refs.
Pd–Cu–Pt/ $\gamma$ - $Al_2O_3$	Nano	95	2.2%	–	Gao et al. (2004)
Pd/ $\gamma$ - $Al_2O_3$	Nano	17.9	2.65%	8.2%	Zhang et al. (2003)
Pd–Cu/ $\gamma$ - $Al_2O_3$	Nano	100	4.31%	94%	Zhang et al. (2003)
Cu–N–C-800	Single atom	100	78.05%	21.82%	Zhu et al. (2020)
Active sepiolite	–	100	–	–	Öztürk et al. (2004)
Activated red mud	–	75	–	–	Cengeloglu et al. (2006)
NZVI–N	Nano	83.5	16.7%	–	Liu et al. (2012)
Sn–Pd@ZSM-5	Nano	100	–	88%	Hamid et al. (2016)
Al alloys particles	Particle	100	80%	–	Bao et al. (2017)
NF–Cu/Pd	Nano	96.4	–	65.4%	Shen et al. (2020)
Pd–Sn@ACF	Nano	97.2	9.3%	37%	Tada et al. (2004)
Co–CNP	Single atom	100	97%–FE	–	Li et al. (2022a, b)
Pd–Cu/Fe	Nano	100	–	28.9%	Liou et al. (2009)
Pd/Cu@NaY	Nano	100	10%	94%	Soares et al. (2015)
Pd–Cu–SAAs	Alloy	42	–	94%	Wu et al. (2023)
Pd–Cu–N–BC	Single atom	100	33.24%	72.32%	This study

## 4 Conclusions

A 3D electrocatalytic reaction system was developed for electrocatalytic reduction of nitrate by using Pd–Cu-N-BC with the best nitrate removal and the high generation of N<sub>2</sub> about 100% and 72.32%, respectively. In the three-dimensional electrocatalytic reduction system, the synergistic effect of Pd and Cu can enhance the reduction of nitrate and promote the production of nitrogen.

The Pd and Cu metal atoms were successfully loaded and uniformly dispersed in the biochar lattice by impregnation, calcination and reduction methods. Heteroatom doping (such as N, P, S, and B. etc.) could modulate the electronic structure of Pd and Cu sites in the biochar lattice at the atomic level and enhance the electrocatalytic reduction of nitrate.

The synergy between Pd and Cu could promote the nitrate reduction into N<sub>2</sub>, and the active sites around the Pd atoms would provide more energy for the N<sub>2</sub>O\* to combine with NO\* to generate N<sub>2</sub>, which could easily escape from the electrolyte because of its inertness and poor solubility. Corresponding to experimental results, Pd and Cu dual metal atoms can cooperate to accomplish the electrocatalytic reduction of nitrate.

### Acknowledgements

We greatly appreciate the suggestions from four reviewers and editors, and we thank the Huasuan institution and Xueyanhui institution for the XAS characterization and the DFT calculation respectively in our research.

### Author contributions

LHZ: methodology, formal analysis, investigation, writing-original draft, visualization. YQW and YD: investigation and experiment, methodology, ZQZ and YNZ: conceptualization, writing-review & editing, validation, funding acquisition. MNL and HD: investigation, formal analysis. All author(s) read and approved the final manuscript.

### Funding

This work was financially supported by the National Natural Science Foundation of China (Nos. 51978188, 42063003, 52160017), the Chinese Postdoctoral Science Foundation (2019M650869), the Research Foundation of Guangxi Key Laboratory of Environmental Pollution Control Theory and Technology (Guikeneng 2301Z001) the Special Fundation for Guangxi Distinguished Experts and Program for High Level Innovation Team and Outstanding Scholar of Universities in Guangxi (GuiCaiJiaoHan [2018]319).

### Availability of data and materials

The datasets used or analyzed during the current study are available from the corresponding author on reasonable request.

### Declarations

#### Ethics approval and consent to participate

The manuscript is approved by all authors for publication. I would like to declare on behalf of my co-authors that the work described is original research that has not been published previously, and not under consideration for publication elsewhere.

#### Consent for publication

If the manuscript is accepted, we are willing to transfer the publishing rights to this manuscript.

### Competing interests

The authors declare that they have no known competing financial interests or personal relationships that could have appeared to influence the work reported in this paper.

### Author details

<sup>1</sup>College of Environmental Science and Engineering, Guilin University of Technology, Guilin 541006, People's Republic of China. <sup>2</sup>Guangxi Key Laboratory of Environmental Pollution Control Theory and Technology, Guilin 541006, People's Republic of China. <sup>3</sup>Collaborative Innovation Center for Water Pollution Control and Water Safety in Karst Area, Guilin University of Technology, Guilin 541006, People's Republic of China. <sup>4</sup>Key Laboratory of Drinking Water Science and Technology, Research Center for Eco-Environmental Sciences, Chinese Academy of Sciences, Beijing 100035, People's Republic of China.

Received: 20 September 2023 Revised: 20 December 2023 Accepted: 23 December 2023

Published online: 15 January 2024

### References

- Bao ZS, Hu Q, Qi WK, Tang Y, Wang W, Wan PY, Chao JB, Yang XJ (2017) Nitrate reduction in water by aluminum alloys particles. *J Environ Manage* 196:666–673. <https://doi.org/10.1016/j.jenvman.2017.03.080>
- Carey RO, Migliaccio KW, Brown MT (2011) Nutrient discharges to biscayne bay, Florida: trends, loads, and a pollutant index. *Sci Total Environ* 409(3):530–539. <https://doi.org/10.1016/j.scitotenv.2010.10.029>
- Casella IG, Gatta M (2004) Electrochemical reduction of NO<sub>3</sub><sup>-</sup> and NO<sub>2</sub><sup>-</sup> on a composite copper thallium electrode in alkaline solutions. *J Electroanal Chem* 568:183–188. <https://doi.org/10.1016/j.jelechem.2004.01.021>
- Cengeloglu Y, Tor A, Ersoz M, Arslan G (2006) Removal of nitrate from aqueous solution by using red mud. *Sep Purif Technol* 51:374–378. <https://doi.org/10.1016/j.seppur.2006.02.020>
- Chen F, Jiang X, Zhang L, Lang R, Qiao B (2018a) Single-atom catalysis: bridging the homo- and heterogeneous catalysis. *Chinese J Catal* 39(5):893–898. [https://doi.org/10.1016/S1872-2067\(18\)63047-5](https://doi.org/10.1016/S1872-2067(18)63047-5)
- Chen X, Oh W-D, Hu Z-T, Sun Y-M, Webster RD, Li S-Z, Lim T-T (2018b) Enhancing sulfacetamide degradation by peroxymonosulfate activation with N-doped graphene produced through delicately-controlled nitrogen functionalization via tweaking thermal annealing processes. *Appl Catal B* 225:243–257. <https://doi.org/10.1016/j.apcatb.2017.11.071>
- Chen T, Liu T, Ding T, Pang BB, Wang L, Liu XK, Shen XY, Wang SC, Wu D, Liu D, Cao LL, Luo QQ, Zhang W, Zhu WK, Yao T (2021a) Surface oxygen injection in tin disulfide nanosheets for efficient CO<sub>2</sub> electroreduction to formate and syngas. *Nano-Micro Letters* 13(1):189. <https://doi.org/10.1007/s40820-021-00703-6>
- Chen T, Liu T, Shen XY, Zhang W, Ding T, Wang L, Liu XK, Cao LL, Zhu WK, Li YF, Yao T (2021b) Synergistically electronic tuning of metalloid CdSe nanorods for enhanced electrochemical CO<sub>2</sub> reduction. *Sci China Mater* 64(12):2997–3006. <https://doi.org/10.1007/s40843-021-1696-x>
- Chen J-W, Hsieh S-H, Wong S-S, Chiu Y-C, Shiu H-W, Wang C-H, Yang Y-W, Hsu Y-J, Convertino D, Coletti C, Heun S, Chen C-H, Wu C-L (2022a) Hydrogen spillover and storage on graphene with single-site Ti catalysts. *ACS Energy Lett* 7(7):2297–2303. <https://doi.org/10.1021/acsenerylett.2c00941>
- Chen T, Liu T, Pang BB, Ding T, Zhang W, Shen XY, Wu D, Wang L, Liu XK, Luo QQ, Zhu WK, Yao T (2022b) Actinide-uranium single-atom catalysis for electrochemical nitrogen fixation. *Sci Bull* 67(19):2001–2012. <https://doi.org/10.1016/j.scib.2022.09.001>
- Chen T, Dong HH, Liu T, Zhou L, Fu DJ, Pang BB, Lian J, Ding T, Zhang W, He R, Zhu WK (2023) Amplified single-atom U-O interfacial effect originated from U 5f-O 2p hybridization over UOx/GO for enhanced nitrogen reduction reaction. *Inorg Chem* 62(22):8615–8625. <https://doi.org/10.1021/acs.inorgchem.3c00637>
- Cheng H, Scott K, Christensen P (2005) Application of a solid polymer electrolyte reactor to remove nitrate ions from wastewater. *J Appl Electrochem* 35(6):551–560. <https://doi.org/10.1007/s10800-005-1519-9>
- Choi CH, Kim M, Kwon HC, Cho SJ, Yun S, Kim HT, Mayrhofer KJ, Kim H, Choi M (2016) Tuning selectivity of electrochemical reactions by atomically

- dispersed platinum catalyst. *Nat Commun* 7:10922. <https://doi.org/10.1038/ncomms10922>
- Daiyan R, Tran-Phu T, Kumar P, Iputera K, Tong Z, Leverett J, Khan MHA, Esmailpour AA, Jalili A, Lim M (2021) Nitrate reduction to ammonium: from CuO defect engineering to waste NO<sub>x</sub>-to-NH<sub>3</sub> economic feasibility. *Energy Environ Sci* 14(6):3588–3598. <https://doi.org/10.1039/d1ee00594d>
- Dima GE, de Vooyes ACA, Koper MTM (2003) Electrocatalytic reduction of nitrate at low concentration on coinage and transition-metal electrodes in acid solutions. *J Electroanal Chem* 554:15–23. [https://doi.org/10.1016/S0022-0728\(02\)01443-2](https://doi.org/10.1016/S0022-0728(02)01443-2)
- Duan X, Sun H, Wang Y, Kang J, Wang S (2015) N-doping-induced nonradical reaction on single-walled carbon nanotubes for catalytic phenol oxidation. *ACS Catal* 5(2):553–559. <https://doi.org/10.1021/cs5017613>
- Fadhullah W, Yacob NS, Syakir MI, Muhammad SA, Yue FJ, Li SL (2020) Nitrate sources and processes in the surface water of a tropical reservoir by stable isotopes and mixing model. *Sci Total Environ* 700:134517. <https://doi.org/10.1016/j.scitotenv.2019.134517>
- Gao JF, Xu CY, Wang JF, Zhuang YY (2004) Catalytic reduction of nitrate in water over Pd-Cu-Pt/γ-Al<sub>2</sub>O<sub>3</sub> Catalyst. *Chin J Catal* 25(11):869–872. <https://doi.org/10.3321/j.issn:0253-9837.2004.11.006>. (in Chinese)
- Gao J, Jiang B, Ni C, Qi Y, Zhang Y, Oturan N, Oturan MA (2019) Non-precious Co<sub>3</sub>O<sub>4</sub>-TiO<sub>2</sub>/Ti cathode based electrocatalytic nitrate reduction: Preparation, performance and mechanism. *Appl Catal B* 254:391–402. <https://doi.org/10.1016/j.apcatb.2019.05.016>
- Ghafari S, Hasan M, Aroua MK (2008) Bio-electrochemical removal of nitrate from water and wastewater—a review. *Bioresour Technol* 99(10):3965–3974. <https://doi.org/10.1016/j.biortech.2007.05.026>
- Guo X, Fang G, Li G, Ma H, Fan H, Yu L, Ma C, Wu X, Deng D, Wei M, Tan D, Si R, Zhang S, Li J, Sun L, Tang Z, Pan X, Bao X (2014) Direct, nonoxidative conversion of methane to ethylene, aromatics, and hydrogen. *Science* 344(6184):616–619. <https://doi.org/10.1126/science.1253150>
- Guo Y, Zeng Z, Zhu Y, Huang Z, Cui Y, Yang J (2018) Catalytic oxidation of aqueous organic contaminants by persulfate activated with sulfur-doped hierarchically porous carbon derived from thiophene. *Appl Catal B* 220:635–644. <https://doi.org/10.1016/j.apcatb.2017.08.073>
- Hamid S, Kumar MA, Lee W (2016) Highly reactive and selective Sn-Pd bimetallic catalyst supported by nanocrystalline ZSM-5 for aqueous nitrate reduction. *Appl Catal B: Environ* 187:37–46. <https://doi.org/10.1016/j.apcatb.2016.01.035>
- Ho SH, Chen YD, Li R, Zhang C, Ge Y, Cao G, Ma M, Duan X, Wang S, Ren NQ (2019) N-doped graphitic biochars from C-phycoerythrin extracted Spirulina residue for catalytic persulfate activation toward nonradical disinfection and organic oxidation. *Water Res* 159:77–86. <https://doi.org/10.1016/j.watres.2019.05.008>
- Hoagland B, Schmidt C, Russo TA, Adams R, Kaye J (2019) Controls on nitrogen transformation rates on restored floodplains along the Cosumnes River, California. *Sci Total Environ* 649:979–994. <https://doi.org/10.1016/j.scitotenv.2018.08.379>
- Holmes DE, Dang Y, Smith JA (2019) Nitrogen cycling during wastewater treatment. *Adv App Microbiol* 106:113–192. <https://doi.org/10.1016/b.s.a.2018.10.003>
- Hwang YH, Kim DG, Shin HS (2011) Mechanism study of nitrate reduction by nano zero valent iron. *J Hazard Mater* 185(2–3):1513–1521. <https://doi.org/10.1016/j.jhazmat.2010.10.078>
- Ines M, Soares M, Abeliovich A (1998) Wheat straw as substrate for water denitrification. *Water Res* 32(12):3790–3794. [https://doi.org/10.1016/S0043-1354\(98\)00136-5](https://doi.org/10.1016/S0043-1354(98)00136-5)
- Jin LM, You SJ, Duan XG, Yao Y, Yang JM, Liu YB (2022a) Peroxymonosulfate activation by Fe<sub>3</sub>O<sub>4</sub>-MnO<sub>2</sub>/CNT nanohybrid electroactive filter towards ultrafast micropollutants decontamination: performance and mechanism. *J Hazard Mater* 423:127111. <https://doi.org/10.1016/j.jhazmat.2021.127111>
- Jin LM, You SJ, Ren NQ, Ding B, Liu YB (2022b) Mo vacancy-mediated activation of peroxymonosulfate for ultrafast micropollutant removal using an electrified MXene filter functionalized with Fe single atoms. *Environ Sci Tech* 56(16):11750–11759. <https://doi.org/10.1021/acs.est.2c03904>
- Jin XJ, Liu RR, Wang HF, Han L, Qiu MQ, Hu BW (2022c) Functionalized porous nanoscale Fe<sub>3</sub>O<sub>4</sub> particles supported biochar from peanut shell for Pb(II) ions removal from landscape wastewater. *Environ Sci Pollut R* 29(25):37159–37169. <https://doi.org/10.1007/s11356-021-18432-z>
- Katsounaris I, Kyriacou G (2008) Influence of nitrate concentration on its electrochemical reduction on tin cathode: identification of reaction intermediates. *Electrochim Acta* 53(17):5477–5484. <https://doi.org/10.1016/j.electacta.2008.03.018>
- Khan Z, Yang XJ, Fu Y, Joseph S, Khan MN, Khan MA, Alam I, Shen H (2023) Engineered biochar improves nitrogen use efficiency via stabilizing soil water-stable macroaggregates and enhancing nitrogen transformation. *Biochar* 5(1):52. <https://doi.org/10.1007/s42773-023-00252-8>
- Knobloch L, Salna B, Hogan A, Postle J, Anderson H (2000) Blue babies and nitrate contaminated well water. *Environ Health Persp* 108:675–678. <https://doi.org/10.1289/ehp.00108675>
- Koparal AS, Ögütveren ÜB (2002) Removal of nitrate from water by electroreduction and electrocoagulation. *J Hazard Mater* 89:83–94. [https://doi.org/10.1016/S0304-3894\(01\)00301-6](https://doi.org/10.1016/S0304-3894(01)00301-6)
- Koter S, Chojnowska P, Szykiewicz K, Koter I (2015) Batch electro dialysis of ammonium nitrate and sulfate solutions. *J Membrane Sci* 496:219–228. <https://doi.org/10.1016/j.memsci.2015.08.064>
- Kumar H, Ganesan SP, Bordoloi S, Sreedeeep S, Lin P, Mei G, Garg A, Sarmah AK (2019) Erodibility assessment of compacted biochar amended soil for geo-environmental applications. *Sci Total Environ* 672:698–707. <https://doi.org/10.1016/j.scitotenv.2019.03.417>
- Lang R, Li T, Matsumura D, Miao S, Ren Y, Cui YT, Tan Y, Qiao B, Li L, Wang A, Wang X, Zhang T (2016) Hydroformylation of olefins by a rhodium single-atom catalyst with activity comparable to RhCl(PPh<sub>3</sub>)<sub>3</sub>. *Angew Chem Int Edit* 55(52):16054–16058. <https://doi.org/10.1002/anie.201607885>
- Li C, Wu M, Liu R (2019) High-performance bifunctional oxygen electrocatalysts for zinc-air batteries over mesoporous Fe/Co-NC nanofibers with embedding FeCo alloy nanoparticles. *Appl Catal B* 244:150–158. <https://doi.org/10.1016/j.apcatb.2018.11.039>
- Li X, Rong H, Zhang J, Wang D, Li Y (2020) Modulating the local coordination environment of single-atom catalysts for enhanced catalytic performance. *Nano Res* 13(7):1842–1855. <https://doi.org/10.1007/s12274-020-2755-3>
- Li J, Li M, An N, Zhang S, Song Q, Yang Y, Li J, Liu X (2022a) Boosted ammonium production by single cobalt atom catalysts with high faradic efficiencies. *P Natl Acad Sci USA* 119(29):e2123450119. <https://doi.org/10.1073/pnas.2123450119>
- Li JC, Li M, An N, Zhang S, Song QN, Yang YL, Li J, Liu X (2022b) Boosted ammonium production by single cobalt atom catalysts with high faradic efficiencies. *P Natl Acad Sci USA* 119(29):e2123450119. <https://doi.org/10.1073/pnas.2123450119>
- Liang B, Kang F, Yao S, Zhang K, Wang Y, Chang M, Lyu Z, Zhu T (2021a) Exploration and verification of the feasibility of the sulfur-based autotrophic denitrification integrated biomass-based heterotrophic denitrification systems for wastewater treatment: from feasibility to application. *Chemosphere* 287:131998. <https://doi.org/10.1016/j.chemosphere.2021.131998>
- Liang LP, Xi FF, Tan WS, Meng X, Hu BW, Wang XK (2021b) Review of organic and inorganic pollutants removal by biochar and biochar-based composites. *Biochar* 3(3):255–281. <https://doi.org/10.1007/s42773-021-00101-6>
- Liou YH, Lin CJ, Weng SC, Ou HH, Lo SL (2009) Selective decomposition of aqueous nitrate into nitrogen using iron deposited bimetallics. *Environ Sci & Technol* 43(7):2482–2488. <https://doi.org/10.1021/es802498k>
- Liu HB, Chen TH, Chang DY, Liu Y, He HP, Yuan P, Frost R (2012) Nitrate reduction over nanoscale zero-valent iron prepared by hydrogen reduction of goethite. *Mater Chem Phys* 133:205–211. <https://doi.org/10.1016/j.matchemphys.2012.01.008>
- Liu P, Zhao Y, Qin R, Mo S, Chen G, Gu L, Chevrier DM, Zhang P, Guo Q, Zang D, Wu B, Fu G, Zheng N (2016) Photochemical route for synthesizing atomically dispersed palladium catalysts. *Science* 352(6287):797–801. <https://doi.org/10.1126/science.aaf5251>
- Liu G, Robertson AW, Li MM, Kuo WCH, Darby MT, Muhieddine MH, Lin YC, Suenaga K, Stamatakis M, Warner JH, Tsang SCE (2017) MoS<sub>2</sub> monolayer catalyst doped with isolated Co atoms for the hydrodeoxygenation reaction. *Nat Chem* 9(8):810–816. <https://doi.org/10.1038/nchem.2740>
- Liu H, Lang X, Zhu C, Timoshenko J, Ruscher M, Bai L, Guijarro N, Yin H, Peng Y, Li J, Liu Z, Wang W, Cuenya BR, Luo J (2022) Efficient electrochemical nitrate reduction to ammonia with copper-supported rhodium cluster and single-atom catalysts. *Angew Chem Int Edit* 61(23):e202202556. <https://doi.org/10.1002/anie.202202556>
- Liu FL, Wang SS, Zhao CF, Hu BW (2023) Constructing coconut shell biochar/MXenes composites through self-assembly strategy to enhance U(VI) and



- Cs(I) immobilization capability. *Biochar* 5(1):31. <https://doi.org/10.1007/s42773-023-00231-z>
- Nirmala C, Bisht MS, Bajwa HK, Santosh O (2018) Bamboo: a rich source of natural antioxidants and its applications in the food and pharmaceutical industry. *Trends Food Sci Tech* 77:91–99. <https://doi.org/10.1016/j.tifs.2018.05.003>
- Niu H, Zhang Z, Wang X, Wan X, Shao C, Guo Y (2020) Theoretical insights into the mechanism of selective nitrate-to-ammonia electroreduction on single-atom catalysts. *Adv Funct Mater* 31(11):2008533. <https://doi.org/10.1002/adfm.202008533>
- Ovez B, Mergaert J, Saglam M (2006) Biological denitrification in drinking water treatment using the seaweed *Gracilaria verrucosa* as carbon source and biofilm carrier. *Water Environ Res* 78(4):430–434. <https://doi.org/10.2175/106143006X98822>
- Öztürk N, Bektaş TE (2004) Nitrate removal from aqueous solution by adsorption onto various materials. *J Hazard Mater* 112(1–2):155–162. <https://doi.org/10.1016/j.jhazmat.2004.05.001>
- Panee J (2015) Potential medicinal application and toxicity evaluation of extracts from bamboo plants. *J Med Plants Res* 9(23):681. <https://doi.org/10.5897/jmpr2014.5657>
- Pérez-Gallent E, Figueiredo MC, Katsounaros I, Koper MT (2017) Electrocatalytic reduction of nitrate on copper single crystals in acidic and alkaline solutions. *Electrochim Acta* 227:77–84. <https://doi.org/10.1016/j.electacta.2016.12.147>
- Pintar A, Batista J, Mušević I (2004) Palladium-copper and palladium-tin catalysts in the liquid phase nitrate hydrogenation in a batch-recycle reactor. *Appl Catal b: Environ* 52(1):49–60. <https://doi.org/10.1016/j.apcatb.2004.02.019>
- Prüsse U, Hähnlein M, Daum J, Vorlop K-D (2000) Improving the catalytic nitrate reduction. *Catal Today* 55(1–2):79–90. [https://doi.org/10.1016/S0920-5861\(99\)00228-X](https://doi.org/10.1016/S0920-5861(99)00228-X)
- Qiao B, Wang A, Yang X, Allard LF, Jiang Z, Cui Y, Liu J, Li J, Zhang T (2011) Single-atom catalysis of CO oxidation using Pt<sub>1</sub>/FeO<sub>x</sub>. *Nat Chem* 3(8):634–641. <https://doi.org/10.1038/nchem.1095>
- Qiu H-J, Liu L, Mu Y-P, Zhang H-J, Wang Y (2015) Designed synthesis of cobalt-oxide-based nanomaterials for superior electrochemical energy storage devices. *Nano Res* 8(2):321–339. <https://doi.org/10.1007/s12274-014-0589-6>
- Qiu MQ, Hu BW, Chen ZS, Yang H, Zhuang L, Wang XK (2021) Challenges of organic pollutant photocatalysis by biochar-based catalysts. *Biochar* 3(2):117–123. <https://doi.org/10.1007/s42773-021-00098-y>
- Qiu MQ, Liu LJ, Ling Q, Cai YW, Yu SJ, Wang SQ, Fu D, Hu BW, Wang XK (2022) Biochar for the removal of contaminants from soil and water: a review. *Biochar* 4(1):19. <https://doi.org/10.1007/s42773-022-00146-1>
- Ruangchainikom C, Liao CH, Anotai J, Lee MT (2006) Characteristics of nitrate reduction by zero-valent iron powder in the recirculated and CO<sub>2</sub>-bubbled system. *Water Res* 40(2):195–204. <https://doi.org/10.1016/j.watres.2005.09.047>
- Shen ZH, Liu DR, Peng GG, Ma YH, Li JS, Shi JL, Peng JB, Ding LJ (2020) Electrocatalytic reduction of nitrate in water using Cu/Pd modified Ni foam cathode: high nitrate removal efficiency and N<sub>2</sub>-selectivity. *Sep Purif Technol* 241:116743. <https://doi.org/10.1016/j.seppur.2020.116743>
- Shin H, Jung S, Bae S, Lee W, Kim H (2014) Nitrite reduction mechanism on a Pd surface. *Environ Sci Technol* 48(21):12768–12774. <https://doi.org/10.1021/es503772x>
- Silva CP, Pereira D, Calisto V, Martins MA, Otero M, Esteves VI, Lima DL (2021) Biochar-TiO<sub>2</sub> magnetic nanocomposites for photocatalytic solar-driven removal of antibiotics from aquaculture effluents. *J Environ Manage* 294:112937. <https://doi.org/10.1016/j.jenvman.2021.112937>
- Soares OSGP, Marques L, Freitas CMAS, Fonseca AM, Neves IC (2015) Mono and bimetallic NaY catalysts with high performance in nitrate reduction in water. *Chem Eng J* 281:411–417. <https://doi.org/10.1016/j.cej.2015.06.093>
- Souza-Garcia J, Ticianelli E, Climent V, Felici J (2012) Mechanistic changes observed in heavy water for nitrate reduction reaction on palladium-modified Pt (hkl) electrodes. *Chem Sci* 3(10):3063–3070. <https://doi.org/10.1039/C2SC20490H>
- Su L, Li K, Zhang H, Fan M, Ying D, Sun T, Wang Y, Jia J (2017) Electrochemical nitrate reduction by using a novel Co<sub>3</sub>O<sub>4</sub>/Ti cathode. *Water Res* 120:1–11. <https://doi.org/10.1016/j.watres.2017.04.069>
- Sun E, Zhang Y, Xiao Q, Li H, Qu P, Yong C, Wang B, Feng Y, Huang H, Yang L, Hunter C (2022) Formable porous biochar loaded with La-Fe(hydr)oxides/montmorillonite for efficient removal of phosphorus in wastewater: process and mechanisms. *Biochar* 4(1):53. <https://doi.org/10.1007/s42773-022-00177-8>
- Tada K, Kawaguchi T, Shimazu K (2004) High electrocatalytic performance of Pd/Sn/Au electrodes for nitrate reduction. *J Electroanal Chem* 572:93–99. <https://doi.org/10.1016/j.jelechem.2004.06.004>
- Thotagamuge R, Kooh MRR, Mahadi AH, Lim CM, Abu M, Jan A, Hanipah AHA, Khiong YY, Shofry A (2021) Copper modified activated bamboo charcoal to enhance adsorption of heavy metals from industrial wastewater. *Environ Nanotech Monitor & Manag* 16:100562. <https://doi.org/10.1016/j.enmm.2021.100562>
- Vilé G, Albani D, Nachttegaal M, Chen Z, Dontsova D, Antonietti M, López N, Pérez-Ramírez J (2015) A stable single-site palladium catalyst for hydrogenations. *Angew Chem Int Edit* 54(38):11265–11269. <https://doi.org/10.1002/anie.201505073>
- Wang Y (2006) Electrochemical-chemical catalytic reduction of nitrate in water. Doctoral Dissertation of Graduate School of Chinese Academy of Sciences. <http://159.226.240.226/handle/311016/115>. (in Chinese)
- Wang J, Chu L (2016) Biological nitrate removal from water and wastewater by solid-phase denitrification process. *Biotechnol Adv* 34(6):1103–1112. <https://doi.org/10.1016/j.biotechadv.2016.07.001>
- Wang Q, Wang W, Yan B, Shi W, Cui F, Wang C (2017) Well-dispersed Pd-Cu bimetallics in TiO<sub>2</sub> nanofiber matrix with enhanced activity and selectivity for nitrate catalytic reduction. *Chem Eng J* 326:182–191. <https://doi.org/10.1016/j.cej.2017.05.110>
- Ward MH, deKok TM, Levallois P, Brender J, Gulis G, Nolan BT, VanDerslice J (2005) Workgroup report: drinking-water nitrate and health—recent findings and research needs. *Environ Health Persp* 113(11):1607–1614. <https://doi.org/10.1289/ehp.8043>
- Wei Z, Senbayram M, Zhao X, Li C, Jin K, Wu M, Rahman MM, Shan J, Yan X (2022) Biochar amendment alters the partitioning of nitrate reduction by significantly enhancing DNRA in a paddy field. *Biochar* 4(1):44. <https://doi.org/10.1007/s42773-022-00166-x>
- Weon S, Huang D, Rigby K, Chu C, Wu X, Kim J-H (2020) Environmental materials beyond and below the nanoscale: single-atom catalysts. *ACS EST Eng* 1(2):157–172. <https://doi.org/10.1021/acsestengg.0c00136>
- Wu YQ, Zhu ZQ, Zhang LH, Dong Y, Liu SS, Zhu YN, Li YH (2022) Electrocatalytic reduction of nitrate on Pd/Cu bamboo biochar particle. *Res Environ Sci* 35(9):2156–2164. <https://doi.org/10.13198/j.issn.1001-6929.2022.04.03>. (in Chinese)
- Wu XH, Nazemi M, Gupta S, Chismar A, Hong K, Jacobs H, Zhang WQ, Rigby K, Hedtke T, Wang QX, Stavitski E, Wong MS, Muhich C, Kim J-H (2023) Contrasting capability of single atom palladium for thermocatalytic versus electrocatalytic nitrate reduction reaction. *ACS Catal* 13:6804–6812. <https://doi.org/10.1021/acscatal.3c01285>
- Xu L, Wu C, Liu P, Bai X, Du X, Jin P, Yang L, Jin X, Shi X, Wang Y (2020a) Peroxymonosulfate activation by nitrogen-doped biochar from sawdust for the efficient degradation of organic pollutants. *Chem Eng J* 387:124065. <https://doi.org/10.1016/j.cej.2020.124065>
- Xu L, Fu B, Sun Y, Jin P, Bai X, Jin X, Shi X, Wang Y, Nie S (2020b) Degradation of organic pollutants by Fe/N co-doped biochar via peroxymonosulfate activation: synthesis, performance, mechanism and its potential for practical application. *Chem Eng J* 400:125870. <https://doi.org/10.1016/j.cej.2020.125870>
- Xu Y, Ren K, Ren T, Wang M, Liu M, Wang Z, Li X, Wang L, Wang H (2021) Cooperativity of Cu and Pd active sites in CuPd aerogels enhances nitrate electroreduction to ammonia. *Chem Commun* 57(61):7525–7528. <https://doi.org/10.1039/D1CC02105B>
- Yang M, Liu J, Lee S, Zugic B, Huang J, Allard LF, Flytzani-Stephanopoulos M (2015) A common single-site Pt(II)-O(OH) x-species stabilized by sodium on "active" and "inert" supports catalyzes the water-gas shift reaction. *J Am Chem Soc* 137(10):3470–3473. <https://doi.org/10.1021/ja513292k>
- Yang S, Kim J, Tak YJ, Soon A, Lee H (2016) Single-atom catalyst of platinum supported on titanium nitride for selective electrochemical reactions. *Angew Chem Int Edit* 55(6):2058–2062. <https://doi.org/10.1002/anie.201509241>
- Zhai Y, Zhao X, Teng Y, Li X, Zhang J, Wu J, Zuo R (2017) Groundwater nitrate pollution and human health risk assessment by using HHRA model in an agricultural area, NE China. *Ecotox Environ Safe* 137:130–142. <https://doi.org/10.1016/j.ecoenv.2016.11.010>

- Zhang Y, Chen YX, Zhang HY (2003) Catalytic reduction of nitrate in water over Pd-Cu/ $\gamma$ -Al<sub>2</sub>O<sub>3</sub> Catalyst. *Chinese J Catal* 24(4):270–274. <https://doi.org/10.3321/j.issn:0253-9837.2003.04.008>. (in Chinese)
- Zhang Z, Xu Y, Shi W, Wang W, Zhang R, Bao X, Zhang B, Li L, Cui F (2016) Electrochemical-catalytic reduction of nitrate over Pd-Cu/ $\gamma$ -Al<sub>2</sub>O<sub>3</sub> catalyst in cathode chamber: enhanced removal efficiency and N<sub>2</sub> selectivity. *Chem Eng J* 290:201–208. <https://doi.org/10.1016/j.cej.2016.01.063>
- Zhang Z, Shi W, Wang W, Xu Y, Bao X, Zhang R, Zhang B, Guo Y, Cui F (2018) Interfacial electronic effects of palladium nanocatalysts on the by-product ammonia selectivity during nitrite catalytic reduction. *Environ Sci Nano* 5(2):338–349. <https://doi.org/10.1039/C7EN00909G>
- Zhang H, Liu Y, Chen T, Zhang J, Zhang J, Lou XW (2019) Unveiling the activity origin of electrocatalytic oxygen evolution over isolated Ni atoms supported on a N-doped carbon matrix. *Adv Mater* 31(48):1904548. <https://doi.org/10.1002/adma.201904548>
- Zhang X, Zhang Y, Shi P, Bi Z, Shan Z, Ren L (2021) The deep challenge of nitrate pollution in river water of China. *Sci Total Environ* 770:144674. <https://doi.org/10.1016/j.scitotenv.2020.144674>
- Zhao X, Li X, Zhang H, Chen X, Xu J, Yang J, Zhang H, Hu G (2022) Atomic-dispersed copper simultaneously achieve high-efficiency removal and high-value-added conversion to ammonia of nitrate in sewage. *J Hazard Mater* 424:127319. <https://doi.org/10.1016/j.jhazmat.2021.127319>
- Zheng WT, Liu YB, Liu FQ, Wang Y, Ren NQ, You SJ (2022) Atomic hydrogen in electrocatalytic systems: generation, identification, and environmental applications. *Water Res* 223:118994. <https://doi.org/10.1016/j.watres.2022.118994>
- Zhu T, Chen Q, Liao P, Duan W, Liang S, Yan Z, Feng C (2020) Single-atom Cu catalysts for enhanced electrocatalytic nitrate reduction with significant alleviation of nitrite production. *Small* 16(49):e2004526. <https://doi.org/10.1002/smll.202004526>